HHS Public Access

Author manuscript

Cell Rep. Author manuscript; available in PMC 2023 October 23.

Published in final edited form as:

Cell Rep. 2023 April 25; 42(4): 112338. doi:10.1016/j.celrep.2023.112338.

Matrix stiffness regulates tumor cell intravasation through expression and ESRP1-mediated alternative splicing of MENA

Wenjun Wang[1], **Paul V. Taufalele**[1], **Martial Millet**[2,3], **Kevin Homsy**[2,3], **Kyra Smart**[1], **Emily D. Berestesky**[1], **Curtis T. Schunk**[1], **Matthew M. Rowe**[1], **Francois Bordeleau**[2,3,4,*], **Cynthia A. Reinhart-King**[1,5,*]

[1]Department of Biomedical Engineering, Vanderbilt University, Nashville, TN 37235, USA

[2]CHU de Québec-Université Laval Research Center (Oncology Division), Québec, QC G1R 3S3, Canada

[3]CHU de Québec-Université Laval Research Center (Oncology Division), Québec, QC G1R 3S3, Canada

[4]Département de biologie moléculaire, de biochimie médicale et de pathologie, Université Laval, Québec, QC G1V 0A6, Canada

[5]Lead contact

SUMMARY

During intravasation, cancer cells cross the endothelial barrier and enter the circulation. Extracellular matrix stiffening has been correlated with tumor metastatic potential; however, little is known about the effects of matrix stiffness on intravasation. Here, we utilize *in vitro* systems, a mouse model, specimens from patients with breast cancer, and RNA expression profiles from The Cancer Genome Atlas Program (TCGA) to investigate the molecular mechanism by which matrix stiffening promotes tumor cell intravasation. Our data show that heightened matrix stiffness increases MENA expression, which promotes contractility and intravasation through focal adhesion kinase activity. Further, matrix stiffening decreases epithelial splicing regulatory protein 1 (ESRP1) expression, which triggers alternative splicing of MENA, decreases the expression of MENA^{11a}, and enhances contractility and intravasation. Altogether, our data indicate that matrix stiffness regulates tumor cell intravasation through enhanced expression and ESRP1-mediated alternative splicing of MENA, providing a mechanism by which matrix stiffness regulates tumor cell intravasation.

In brief

*Correspondence: francois.bordeleau@fmed.ulaval.ca (F.B.), cynthia.reinhart-king@vanderbilt.edu (C.A.R.-K.).

AUTHOR CONTRIBUTIONS

W.W., F.B., and C.A.R.-K. designed research; W.W., P.V.T., M.M., K.S., K.H., and M.M.R. performed the experiments; W.W., M.M., C.T.S., and E.D.B. analyzed data; F.B. and C.A.R.-K. supervised the study, and all authors contributed to writing the manuscript.

DECLARATION OF INTERESTS

The authors declare no competing interests.

SUPPLEMENTAL INFORMATION

Supplemental information can be found online at https://doi.org/10.1016/j.celrep.2023.112338.

Wang et al. show the mechanism wherein ECM stiffness increases expression and ESRP1-mediated alternative splicing of MENA to promote intravasation. As ESRP1 regulates EMT, the findings suggest a link between ECM stiffness and EMT. Furthermore, they also highlight how inhibiting mechanical sensing may aid anti-cancer therapy.

Graphical Abstract

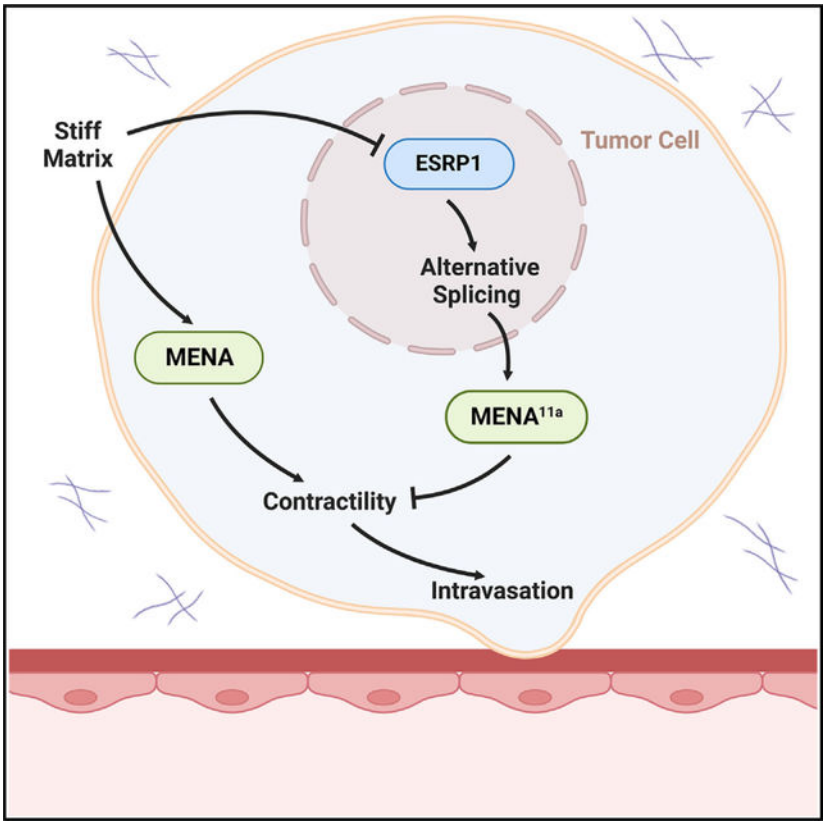

INTRODUCTION

Intravasation is a critical step of metastasis wherein cancer cells cross the endothelial barrier and migrate into the bloodstream.[1] Tumor cell intravasation is co-regulated by many factors within the tumor microenvironment, including communication between different types of cells, proteases, signaling molecules, microenvironmental conditions, and associated tumor vasculature.[1] In addition to these cellular and molecular cues, the extracellular matrix (ECM) is a critical element of the tumor microenvironment.[2] Stiffening of tumor ECM during cancer progression occurs due to increased collagen deposition and crosslinking reactions.[2] This elevated ECM rigidity directly affects multiple cell behaviors, including cell contractility, response to growth factors, and increased cell migration,[3–5] which can further induce a malignant phenotype in nontransformed epithelial cells. Increased matrix stiffness has also been correlated with tumor metastatic potential.[3,4] However, it is still not completely understood how matrix stiffness affects each step leading to tumor metastasis, especially tumor intravasation.

Tumor cells that actively undergo intravasation have been shown to exhibit increased MENA expression.[6] MENA is a member of the Ena/VASP family that regulates actin cytoskeleton dynamics and further controls invadopodia formation during intravasation.[7] MENA is highly upregulated in invasive cancer cells collected from primary tumors and is involved in several motility pathways associated with invasive behaviors and cell-ECM interactions.[8] Furthermore, increased MENA expression is associated with a poor clinical outcome in patients with breast cancer.[8,9] A recent study reported that expression of MENA increases with ECM stiffness.[10] Given the involvement of MENA in both tumor cell intravasation and cell-ECM interactions, we hypothesized that matrix stiffness regulates tumor cell intravasation through MENA.

In addition to changes in overall expression, MENA undergoes alternative splicing during tumor progression resulting in multiple splicing isoforms.[11–13] These splicing isoforms exhibit divergent effects on cytoskeleton dynamics that further modulate the contractility, motility, and intravasation capability of tumor cells.[11–14] For instance, MENA^{11a} inhibits growth-factor-mediated membrane protrusions and attenuates G-actin incorporation to barbed ends of actin filaments, while MENA^{INV} demonstrates an opposite effect.[7,12,15] In addition to regulating intravasation, assessment of MENA splicing isoforms has been suggested as a biomarker for tumor metastasis.[6] A calculated MENA score of total MENA minus MENA^{11a} has been associated with metastasis in breast cancer, where expression of MENA^{11a} is negatively correlated with the metastatic potential of breast tumors.[9,16] Given that alternative splicing of MENA has been implicated in the regulation of both cellular behavior and tumor metastasis, several studies have focused on understanding the mechanism by which MENA alternative splicing is regulated.[7,12,13]

Epithelial-specific splicing factor 1 (ESRP1), an RNA-binding protein, regulates alternative splicing of MENA.[13] ESRP1 is a global regulator of an epithelial splicing regulatory network that regulates alternative splicing events in many genes associated with the reorganization of the actin cytoskeleton and maintenance of cell-cell adhesion, tight junctions, and cellular polarity during the epithelial-to-mesenchymal transition (EMT).[17] Overexpression of ESRP1 and ESRP2 in basal-like breast cancer cells results in upregulation of epithelial cadherin expression, a key marker of the epithelial phenotype.[18] Besides ESRP1-mediated splicing, numerous other transcriptional-factor-mediated events happen during tumor progression.[17] While many of these are believed to favor oncogenesis, the physiological cues that cause alternative splicing events are relatively unclear. A previous study by our group demonstrated that matrix stiffness regulates alternative splicing of fibronectin through increased phosphorylation of splicing factors.[19] As matrix stiffness regulates cell behavior through alternative splicing, and as MENA splicing isoforms play critical roles in cytoskeletal organization, we investigated whether alternative splicing of MENA could be regulated by matrix-stiffness-mediated ESRP1 activity to promote intravasation.

Here, we show that matrix stiffening increases MENA expression and contractility of tumor cells, which leads to increased intravasation. Matrix stiffening also decreased ESRP1 expression and shifted alternative splicing of MENA to downregulate MENA^{11a} expression, while pharmacological inhibition of focal adhesion kinase (FAK) activity reversed this

effect. Using an *in vitro* transwell-based intravasation system polyacrylamide(PA) gels, an *in vivo* mouse model, patient specimens, and RNA expression profiles from The Cancer Genome Atlas (TCGA) program, our study provides direct evidence that matrix stiffness of tumor stroma regulates tumor cell intravasation and alternative splicing of MENA via ESRP1 expression.

RESULTS

Matrix stiffening promotes tumor cell intravasation and MENA expression

Previous studies have shown that ECM stiffening promotes tumor metastasis.[3,20] However, the mechanism by which matrix stiffness regulates tumor cell intravasation, one of the critical steps of metastasis, is still relatively unclear. To address this question, we first tested the correlation between matrix stiffness and tumor cell intravasation with a transwell-based intravasation model adopted from previous studies.[21] Nonenzymatic glycation was utilized to increase the stiffness of collagen matrices from ~180 to ~500 Pa without altering the structure.[22,23] Prior to embedding tumor cells, the formation of a human umbilical vein endothelial cell (HUVEC) monolayer was verified using immunofluorescence staining and a permeability assay. we observed that HUVECs formed VE-cadherin-positive junctions (Figure S1A), and permeability decreased when a HUVEC monolayer existed (Figure S1B). By embedding cells in collagen matrices glycated with different amounts of ribose, we observed that MDA-MB-231 cells within stiff matrices (glycated with 100 mM ribose) exhibited significantly higher intravasation than cells within compliant matrices (unglycated) (Figure 1A).[22] To elucidate the contribution of stiffness-induced migration to the overall phenotype we observed, we next compared the migration speed of MDA-MB-231 embedded in compliant or stiff collagen matrices. Consistent with other studies, we observed that matrix stiffening results in a significant 28% increase in migration speed (Figure S1C).[24] Intriguingly, we also observed that the intravasation index of MDA-MB-231 cells in the stiff collagen matrix was approximately 2-fold higher than that of cells in the compliant matrix. These observations suggest that ECM stiffness increases the intravasation capability of tumor cells besides promoting tumor cell migration.

Noting that MENA contributes to the regulation of tumor cell intravasation, we then determined whether matrix stiffness regulates MENA expression. Western blotting was performed to compare MENA expression of MDA-MB-231 cells seeded on PA gels of 1 or 10 kPa stiffness. We observed that heightened matrix stiffness increased MENA expression (Figures 1B and 1C). This finding was next confirmed *in vivo* using FVB/N-Tg(MMTV-PyVT)634Mul/J (MMTV- PyMT) mice treated with β-aminopropionitrile (BAPN), which inhibits matrix crosslinking enzyme lysyl oxidase (LOX) activity, to produce mice with more compliant tumors.[2,19] As we and others have shown, tumors in mice treated with BAPN are softer. The stiffness of control tumors is around 4,500 Pa, while the stiffness of BAPN-treated tumors is around 3,000 Pa.[2,19,25–27] To confirm that BAPN had no other effect besides inhibiting LOX activity and softening the tumor ECM, we compared cell proliferation *in vivo* and *in vitro* following treatment with or without BAPN. Consistent with previous studies, LOX inhibition decreases the proliferation of tumor cells in vivo (Figure S2A).[28] However, when we investigated the effect of BAPN on MET-1 cells extracted

from MMTV-PyMT mice in vitro, we did not observe any significant difference between cell proliferation or cell area of control- and BAPN-treated cells (Figures S2B and S2C). MENA expression within tumors extracted from MMTV-PyMT mice treated with or without BAPN was assessed via western blotting and immunofluorescence staining (Figures 1D–1G). Stiff tumors (Ctrl) had higher MENA expression than compliant tumors (BAPN). These results indicate that matrix stiffening promotes tumor cell intravasation and increased MENA expression.

Matrix-stiffness-mediated MENA expression regulates tumor cell intravasation

Noting that matrix stiffening promotes both tumor cell intravasation and MENA expression, we next investigated whether MENA plays a role in matrix-stiffness-mediated tumor cell intravasation. MENA knockdown in the MDA-MB-231 cell line was accomplished using short hairpin RNA (shRNA). Knockdown efficiency was confirmed with western blot (Figures 2A and 2B) and quantitative RT-PCR (Figure 2C). Consistent with previous results, tumor cell intravasation was promoted with increasing matrix stiffness, while knockdown of MENA expression significantly decreased the intravasation of cells within both compliant and stiff matrices (Figure 2D). To eliminate the possibility that MENA downregulation influences cell migration, the migration speed of MDA-MB-231 cells embedded in collagen matrix with normal or reduced MENA expression was compared. We did not observe a significant difference between the migration speed of control and shMENA cells (Figure S1C). Previous studies have shown that increasing cell contractility promotes intravasation[29,30] and that MENA regulates tension-sensitive actin cytoskeleton assembly, which plays a critical role in regulating cell contractility.[31] To further investigate the effects of MENA on cell contractility, control MDA-MB-231 cells or MENA knockdown cells were embedded in glycated (stiff) or unglycated (compliant) collagen matrices, and cell contractility was assayed using quantitative polarization microscopy (qPOL). qPOL is a microscopy-based method that provides a linearly proportional readout of cell contractility of 3D cell culture by measuring optical retardance.[32] With qPOL, we observed that cells within stiffer matrices (glycated with 100 mM ribose) exhibited higher contractility compared with cells within more compliant matrices (unglycated) (Figures 2E and 2F). Notably, knockdown of MENA expression significantly decreased the contractility of cells exposed to the stiffer matrix. This result has also been verified using traction force microscopy as described previously.[33] MDA-MB-231 cells with decreased MENA expression had significantly lower cell contractility (Figure S1E). These results indicate that matrix-stiffness-mediated MENA expression regulates the contractility of tumor cells and alters their intravasation capability.

FAK is a key focal adhesion protein involved in cell mechanosensing.[34] When cells attach to a stiff ECM, FAK is recruited to focal adhesions and phosphorylated, initiating downstream signaling cascades and increased cell contractility.[34] To determine the role of the mechanosignaling via FAK in matrix-stiffness-mediated MENA expression and intravasation, we expanded our investigation to assess MENA expression and cell contractility as a function of stiffness-induced FAK activation by inhibiting FAK activation on stiffer matrices. To pharmacologically inhibit FAK, we utilized PF573228, an inhibitor of FAK autophosphorylation at Tyr397.[35] MDA-MB-231 cells on PA gels with 1 or 10

kPa stiffness were treated with either PF573228 (FAKi) or the DMSO vehicle control (Ctrl). MENA expression and cell contractility were assayed with quantitative RT-PCR and qPOL, respectively. While MENA expression increased as a function of substrate stiffness, PF573228 treatment significantly decreased the MENA expression of cells on both compliant and stiff substrates (Figure 2G). Consistent with other studies, cell contractility increased with matrix stiffening and decreased significantly when cells were treated with the FAK inhibitor (Figures 2H and 2I). These data support our hypothesis that matrix stiffness regulates MENA expression and intravasation through FAK-mediated mechanosensory signaling. Taken together, these results demonstrate that matrix stiffening-induced FAK activation is involved in the upregulation of MENA expression, which further promotes the intravasation of tumor cells through increased cell contractility.

Matrix stiffness regulates tumor cell intravasation through alternative splicing of MENA

In addition to increased expression, MENA has also been reported to undergo alternative splicing and generate multiple splicing isoforms during the tumor progression.[11] To test whether matrix stiffness also affects alternative splicing of MENA, MDA-MB-231 cells were seeded on either 1 or 10 kPa PA gels, and the RNA expression of total MENA and $MENA^{11a}$, a splicing isoform that regulates cytoskeletal dynamics and intravasation, was assessed with quantitative RT-PCR. Consistent with previous results, MDA-MB-231 cells on stiff substrates maintained higher total MENA expression than cells on compliant substrates (Figure 3A). Interestingly, we also observed that expression of $MENA^{11a}$ decreased with matrix stiffening (Figure 3B), indicating that alternative splicing of MENA was affected by matrix stiffness.

Besides $MENA^{11a}$, expression of $MENA^{INV}$ and $MENA^{\Delta V6}$, two others of the most-studied MENA isoforms, were also tested. We observed that matrix stiffening did not influence the expression of these isoforms significantly (Figure S3). This result was also verified with an *in vivo* mouse model. Using quantitative RT-PCR, we measured MENA and $MENA^{11a}$ RNA expression in tumors extracted from PyMT mice treated with or without BAPN. Tumors with higher ECM stiffness (Ctrl) showed higher MENA expression but lower $MENA^{11a}$ expression compared with more compliant tumors (BAPN) (Figures 3C and 3D). Thus, we concluded that matrix stiffening shifts both expression and alternative splicing of MENA. Noting that FAK is one mechanism by which mechanical signals are transduced into the cell, we assayed the $MENA^{11a}$ expression level of cells seeded on compliant or stiff PA gel substrates treated with the FAK inhibitor PF573228 to determine if matrix stiffening shifts alternative splicing of MENA through mechanosensitive FAK signaling. The expression of $MENA^{11a}$ decreased with increased matrix stiffness, while inhibition of FAK activity increased $MENA^{11a}$ at both stiffnesses (Figure 3E). These findings suggest that matrix stiffening shifts alternative splicing of MENA and inhibits the expression of $MENA^{11a}$ through FAK-mediated mechanotransduction. Since $MENA^{11a}$ is an isoform that negatively correlates with tumor cell *trans*-endothelial migration potential,[7] we tested whether matrix-stiffness-mediated $MENA^{11a}$ expression regulates tumor cell intravasation. A $MENA^{11a}$ knockdown cell line was generated using shRNA, and the expression of MENA and $MENA^{11a}$ was assayed using quantitative RT-PCR (Figures 3F and 3H). Noting that MENA is involved in the regulation of cell contractility and that different MENA splicing

isoforms exhibit divergent effects on cytoskeleton dynamics and contractility, we next tested whether inhibition of MENA^{11a} influences cell contractility.[14] Cell contractility of control MDA-MB-231 cells or MENA^{11a} knockdown cells embedded in glycated or unglycated collagen matrices was quantified using qPOL. We observed that cells within stiffer matrices (glycated with 100 mM ribose) displayed higher contractility than those within more compliant matrices (unglycated), while inhibition of MENA^{11a} expression increased cell contractility significantly (Figure 3H). As performed for shMENA cells, we compared cell contractility of cells with normal and decreased MENA^{11a} expression using traction force microscopy (TFM). We observed that shMENA^{11a} cells had significantly higher cell contractility compared with control cells (Figure S1E). Intravasation of these cells was also compared using the intravasation-directed transendothelial migration model (iTEM). We found that while all cells exhibited more active intravasation within the stiff matrix, the knockdown of MENA^{11a} resulted in significantly higher intravasation in both stiff and compliant matrices (Figure 3I). To eliminate the possibility that decreased MENA^{11a} influences cell migration, we compared the migration speed of MDA-MB-231 cells with normal or reduced MENA^{11a} expression, and we found no significant difference between these two conditions (Figure S1C). Altogether, these data suggest that increased matrix stiffness shifts alternative splicing of MENA and decreases the expression of MENA^{11a}, which leads to increased intravasation of tumor cells.

ECM stiffness regulates the expression of ESRP1

Our data indicate that matrix stiffness regulates MENA alternative splicing and expression of the MENA^{11a} isoform, and previous studies have demonstrated that ESRP1 regulates the exon inclusion of MENA^{11a}.[18] As such, we determined whether matrix stiffness regulates MENA splicing through decreased ESRP1 expression. MDA-MB-231 cells were seeded on 1 and 10 kPa PA gels and treated with either PF573228 (FAKi) or vehicle control, DMSO (Ctrl). Expression of ESRP1 was assessed with quantitative RT-PCR, immunofluorescence staining, and western blotting. Our results indicate that increased matrix stiffness significantly decreased ESRP1 expression in MDA-MB-231 cells and that FAK inhibition led to a significant increase in ESRP1 expression (Figures 4A–4E). Furthermore, FAK inhibition experiments (Figures 4A–4E) confirmed that this regulation was mediated by FAK-mediated mechanotransduction. Stiffness-mediated expression of ESRP1 was also verified *in vivo* by quantifying ESRP1 expression using quantitative RT-PCR and immunofluorescence staining. Cells extracted from stiffer tumors showed significantly lower ESRP1 expression at the RNA (Figure 4F) and protein levels (Figures 4G and 4H). These results indicate that matrix stiffening inhibits the expression of ESRP1 both *in vitro* and *in vivo*.

Matrix-stiffness-mediated ESRP1 expression regulates alternative splicing of MENA

As we showed that matrix stiffness regulates the alternative splicing of MENA (Figure 3) and that ESRP1 expression responds to ECM stiffening (Figure 4), we next determined whether matrix stiffness regulates alternative splicing of MENA through ESRP1. An MDA-MB-321 cell line overexpressing ESRP1 was generated, and overexpression was confirmed by western blotting (Figures 5A and 5B). Furthermore, we demonstrated that the overall expression of MENA was not changed due to the overexpression of ESRP1 (Figure 5C).

MENA^{11a} isoform expression of either control cells (Ctrl or FUW) or ESRP1 overexpressed cells (ESRP1) seeded on PA gels with 1 or 10 kPa stiffness was assessed with quantitative RT-PCR. Consistent with our previous results (Figures 3A–3D), MENA^{11a} expression decreased as a function of matrix stiffness, while ESRP1 overexpression significantly increased the expression of MENA^{11a} (Figure 5D), indicating that ESRP1 is involved in the regulation of matrix-stiffness-mediated MENA alternative splicing. Given that MENA regulates tumor cell contractility and intravasation, we next determined whether matrix-stiffness-mediated ESRP1 expression contributes to the regulation of tumor cell contractility and intravasation. Control and ESRP1 overexpressed MDA-MB-231 cells were embedded in compliant (nonglycated) or stiff (glycated with 100 mM ribose) collagen matrices. Consistent with our previous experiment (Figures 2E and 2F), qPOL measurements indicated that cells within stiffer matrices exhibited higher contractility compared with cells within more compliant matrices, while overexpression of ESRP1 decreased cell contractility significantly for both conditions (Figure 5E). This result was also confirmed using TFM. MDA-MB-231 cells with ESRP1 overexpression had significantly lower cell contractility (Figure S1E). By utilizing control and ESRP1 overexpressed cells within the iTEM model, we observed that matrix stiffening promoted tumor cell intravasation, while ESRP1 overexpression significantly decreased tumor cell intravasation (Figure 5F). The migration speed of MDA-MB-231 cells with normal or increased ESRP1 expression was compared to eliminate the effect of cell migration, and we did not observe a significant difference between the migration speed of control and ESRP1 overexpression cells (Figure S1C). To further examine if MENA^{11a} is involved in the regulation of tumor cell intravasation as the major downstream effector of ESRP1, we overexpressed ESRP1 in MDA-MB-231 cells transduced with shRNA targeting MENA^{11a}. We verified ESRP1 overexpression via western blot and its effect on MENA and MENA^{11a} expression via qPCR. We observed that overexpression of ESRP1 in shMENA^{11a} cells did not change the expression of MENA or MENA^{11a} (Figures 6A–6D). We further compared cell migration, cell contractility, and intravasation of shMENA^{11a} cells transduced with or without ESRP1 overexpression plasmid. We observed no difference between these two cell lines (Figures 6E, 6F, and S1E). This suggests that matrix stiffness regulates tumor cell intravasation via ESRP1-mediated MENA^{11a} splicing. Altogether, these data suggest that matrix-stiffness-mediated ESRP1 expression decreases MENA^{11a} expression, further increasing tumor cell contractility and intravasation.

Matrix stiffness regulates ESRP1 expression and alternative splicing of MENA within tumors from patients with breast cancer

Our *in vitro* and *in vivo* data indicate that ESRP1 expression responds to ECM stiffening. We next verified this finding within tumor specimens extracted from patients with breast cancer (clinical information in Table S2). Stiffness of tumor stroma was measured using atomic force microscopy (AFM) (Figure 7A), and ESRP1 expression was quantified using immunofluorescence staining (Figures 7B and 7C). Interestingly, we found that ECM stiffness and ESRP1 expression were inversely correlated within patient tumors (Figure 7D). Moreover, a specimen extracted from a stage IV breast tumor (specimen 77704 in Figures 7A–7D) exhibited significantly higher ECM stiffness and lower ESRP1 expression compared with samples extracted from stage I tumors (other specimens in Figures 7A–7D),

suggesting that matrix stiffness and ESRP1 expression are correlated and change with tumor progression. To verify that our findings apply to the general breast cancer population, RNA expression profiles of 1,093 patients with breast cancer from TCGA were utilized to determine whether expression of ESRP1 and MENA^{11a} is correlated with ECM stiffness. Since there are no matrix stiffness measurements associated with these RNA expression profiles, a YAP signature was generated based on the expression of 14 downstream genes of YAP. The YAP/TAZ transcriptional regulation pathway has been found to sense and mediate mechanical cues derived from the cellular microenvironment.[36] Previous findings reveal that signatures of YAP/TAZ activation are significantly overrepresented in the set of genes regulated by high stiffness.[36,37] We calculated the correlation between ESRP1 expression, MENA PSI (percent spliced in), and YAP signature and found that ESRP1 expression was negatively correlated with the YAP signature, indicating that ESRP1 expression within these tumors was negatively correlated with the stiffness of the tumor stroma (Figure 7E). Consistent with our previous data, PSI of MENA^{11a} was also negatively correlated with the YAP signature, which suggests that expression of MENA^{11a} decreased with matrix stiffening (Figure 7F). To verify that our calculation using the YAP signature represents the correlation between matrix stiffness, ESRP1 expression, and MENA splicing faithfully, we tested the correlation between PSI of MENA^{11a} and a set of 15 randomly selected genes. We did not find any significant correlation between the expression of these randomly selected genes and MENA splicing (Figure 7G). The interplay between YAP expression, tumor matrix stiffness, and breast tumor progression is very complex and context dependent.[36,38,39] Thus, to validate that our YAP signature is a reliable approach to represent tumor ECM stiffness, we quantified nuclear YAP/TAZ in both mice and patients' breast tumor tissue sections. Consistent with previous research, we found that nuclear YAP increases with the increase of ECM stiffness (Figure S4).[36] To further prove our hypothesis, we also created an additional gene signature based on the expression of key matrix and matrix-related genes that are known to be overexpressed and involved in tumor stiffening. Similar to what we had obtained with the YAP signature, both ESRP1 expression and PSI of MENA^{11a} were negatively correlated with the matrix signature (Figures 7H–7J). Altogether, these data suggest that the PSI of MENA^{11a} correlates negatively with matrix stiffness, which is represented by the YAP signature. With these data collected from the breast cancer specimens and TCGA database, we confirmed that expression of ESRP1 and MENA^{11a} is negatively correlated with the matrix stiffness of the tumor stroma.

DISCUSSION

While ECM stiffness has been shown to promote tumor progression by regulating numerous tumor cell behaviors, including response to growth factors and cell migration,[3,20] less is known about the role of stiffness in each of the individual steps of the metastatic cascade. Here, we provide direct evidence that matrix stiffness regulates tumor cell intravasation *in vitro* and determine important molecular mediators of stiffness-mediated intravasation. First, our results indicate that increased matrix stiffness upregulates MENA expression in a FAK-dependent manner. This increased MENA expression enhances cell contractility and enhances tumor cell intravasation. In addition to general MENA expression, we show that matrix stiffness regulates alternative splicing of MENA through FAK-mediated ESRP1

expression *in vitro* and *in vivo*. Furthermore, we observe a negative correlation between ECM stiffness and ESRP1 within patient specimens and RNA profiles from TCGA datasets. This human patient correlation is in agreement with our experimental finding that matrix stiffening decreases ESRP1 expression, leading to alternative splicing of MENA, which enhances tumor cell intravasation. Together, these results establish matrix stiffness as an important regulator of tumor cell intravasation by driving the expression and ESRP1-mediated alternative splicing of MENA.

Cell contractility has been shown to increase as a function of matrix stiffness in both 2D and 3D, and highly contractile cells intravasate more efficiently than poorly contractile cells *in vivo*.[29,30,32] Consistent with our previous study, we observed that heightened matrix stiffness increased cell contractility.[32] MENA is a key regulator of tumor cell intravasation and regulates tension-sensitive actin cytoskeleton assembly and cell contractility of the epithelial monolayer *in vitro*.[7,12,15,21,31] Our results show that MENA expression increases proportionally with an increase in matrix stiffness. Additionally, MENA has been shown to regulate cell contractility.[14] As expected, our data show that depletion of MENA prevents the increase of contractility induced by matrix stiffening. This may partly explain why an increase in matrix stiffness promotes tumor cell intravasation in a MENA-dependent manner. However, MENA is not the only protein that regulates cell contractility. There are also other proteins involved in this regulation, such as Rho GTPases and ROCK isoforms.[40] The possibility remains that other proteins are also contributing to the regulation of intravasation via contractility, either in parallel or in concert with the MENA pathway described here. Interestingly, our data also show that inhibition of cell mechanical sensing and contractility decreases MENA expression significantly. Importantly, these findings suggest that there is a bidirectional correlation existing between cell contractility and MENA expression, and this bidirectional relationship directly contributes to matrix-stiffness-mediated intravasation.

Our previous study reports that matrix stiffness regulates alternative splicing of fibronectin.[19] ECM stiffness acts as a regulator of RNA alternative splicing events and promotes alternative splicing of fibronectin.[19] Consistent with that study, our results here indicate that increased matrix stiffness regulates alternative splicing of MENA and decreases expression of MENA^{11a}, while blocking cell mechanical sensing restores MENA^{11a} expression. Since MENA^{11a} and other MENA splicing isoforms regulate actin cytoskeleton organization, we determined the role of MENA^{11a} in cell contractility regulation and showed that inhibition of MENA^{11a} expression increases tumor cell intravasation via increasing contractility.[7,15] Interestingly, in addition to regulating cytoskeleton dynamics, alternative splicing of MENA is also involved in the regulation of tumor progression.[11] MENA^{11a} expression is negatively correlated with the metastatic potential of breast tumors and could be characterized as a biomarker for tumor metastasis.[6,9,16] ECM stiffness has been associated with breast tumor progression and is likely to be different between tumors at different stages.[5,41] Our results provide insight into a possible mechanism by which tumors from different patients maintain different levels of MENA^{11a} expression.

ESRP1 is a regulator of MENA alternative splicing.[13] Overexpression of ESRP1 has been shown to increase MENA^{11a} expression in tumor cells.[13] Our data show that MENA^{11a} expression is negatively correlated with matrix stiffness. These findings suggest that ESRP1

may be sensitive to ECM stiffness. Indeed, we observed that matrix stiffness decreased ESRP1 expression *in vitro* and *in vivo*. Data collected from patient samples and TCGA database also support our findings that demonstrate a strong negative linear correlation between ESRP1 expression and stiffness of the tumor stroma. Given that there is a bidirectional correlation between MENA and cell contractility, we also determined whether ESRP1 is involved in the regulation of cell contractility,[14] and our data confirmed that the matrix stiffness-induced decrease of ESRP1 expression promotes tumor cell contractility. Of note, ESRP1 is a master regulator of alternative splicing events within epithelial cells and controls the splicing of other proteins besides MENA.[13,42,43] Other signaling pathways, such as the formation of invadopodia, contribute to the regulation of tumor cell intravasation besides the mechanism we showed here.[44] Loss of ESRP1 seems to be sufficient to induce an EMT program in breast epithelial cells, mainly by changing alternative splicing.[17,45] Matrix stiffening has been reported to promote EMT in multiple types of tumors.[4,46] Our results show that matrix stiffness regulates ESRP1 expression, suggesting that ESRP1 may play a role in this stiffness-mediated EMT regulation. As such, the mechanism we report here has important ramifications for the fundamental understanding of how ECM stiffness regulates cell behaviors through changes in alternative splicing. Interestingly, previous studies have reported the plasticity of ESRP1 expression during cancer cell invasion and metastasis.[13,43] Cells invading from cancer nests lost expression of ESRPs, while ESRP1 was re-expressed in cancer cells that reached deep into the surrounding stroma and further distal to the lymph nodes.[43] Since mechanical properties, including matrix stiffness, of different tissues are varied,[47] our study may help explain the plasticity of ESRP1 when cells leave a stiff tumor and subsequently colonize a comparatively soft tissue.

Intravasation is an important step of tumor metastasis. Our data suggest that the mechanical properties of the tumor stroma play a critical role in regulating intravasation-related cell behaviors and tumor progression, notably by controlling MENA expression and alternative splicing. We show that blocking cell mechanosensing via pharmacological inhibition of FAK prevents matrix stiffening-induced MENA upregulation, restores ESRP1-mediated alternative splicing of MENA, and decreases intravasation to comparable levels observed from cells seeded on compliant matrices. Mechanical sensing and signaling have been considered potential prognostic markers and anti-tumor therapeutic targets for several years,[48,49] and many FAK inhibitors are currently undergoing clinical trials.[50,51] Our work highlights that interfering with cell mechanical sensing may have broader implications in cancer therapy than previously recognized.

Limitations of the study

The iTEM used in our study has been carefully characterized and applied by both our group and others to investigate tumor cell intravasation.[21,52] However, we acknowledge that this model does not include the complex hemodynamic conditions present in actual tumor vasculature. Previous *in vitro* research has shown that distinct flow-mediated mechanisms regulate tumor cell invasion in lymphatic vessels.[53] Therefore, incorporating blood flow into the experimental model could potentially enhance the investigation of tumor cell intravasation. Furthermore, we relied solely on quantitative RT-PCR to investigate the expression of MENA splicing isoforms, as no antibodies targeting each isoform are

commercially available. However, differences in RNA levels do not always correspond to differences in protein levels. Therefore, it would be valuable to investigate MENA isoforms at the protein level using isoform-specific antibodies once available. Finally, due to the complexity of intravital imaging, we were unable to track and compare tumor cell intravasation rates in real time between stiff and compliant tumors *in vivo*. Future studies employing improved experimental models, novel antibodies, and intravital microscopy imaging may provide further insight into the precise mechanisms underlying how ECM stiffness regulates tumor cell intravasation and MENA splicing.

STAR★METHODS

RESOURCE AVAILABILITY

Lead contact—Further information and requests for resources and reagents should be directed to the lead contact, Dr. Cynthia A. Reinhart-King (cynthia.reinhart-king@vanderbilt.edu).

Materials availability—This study did not generate new unique reagents.

Data and code availability—All data reported in this paper will be shared by the lead contact upon request.

This paper does not report original code.

Any additional information required to reanalyze the data reported in this paper is available from the lead contact upon request.

EXPERIMENTAL MODEL AND SUBJECT DETAILS

Cell culture—Highly metastatic MDA-MB-231 breast adenocarcinoma cells or MET-1 cells extracted from MMTV-PyMT female mice were maintained in DMEM supplemented with 10% FBS (Atlanta Biologicals, Flowery Branch, GA, USA) and 1% penicillin-streptomycin. BAC1.2F5 cells (generously provided by Dr. Richard Stanley, Albert Einstein College of Medicine) were cultured in α-MEM supplemented with 10% FBS, 1% penicillin-streptomycin, and 3000 U/mL of CSF-1 (R&D System, Minneapolis, MN, USA). To produce lentivirus particles, HEK293T cells were cultured in DMEM supplemented with 10% FBS and 1% penicillin-streptomycin. All cells were cultured at 37°C and 5% CO_2. All cell lines were tested and found negative for mycoplasma contamination using a universal mycoplasma detection kit (30–1012K, ATCC). For FAK inhibition studies, cells were treated with 10 μM PF573228.

Mouse studies—FVB/N-Tg(MMTV-PyVT)634Mul/J (MMTV-PyMT) mice were utilized. All mice were maintained following a protocol approved by the Vanderbilt University Institutional Animal Care and Use Committee. Starting at 4 weeks of age, female MMTV-PyMT mice of FVB strain background (Jackson Laboratory, Bar Harbor, ME, USA) were treated with 3 mg/kg body weight b-aminopropionitrile (BAPN; MilliporeSigma) in drinking water.[19] BAPN inhibits the matrix cross-linking enzyme, LOX, and results in more compliant tumors compared to untreated mice.[2] Mice between 11 and 13 weeks old were

sacrificed by CO_2 asphyxiation and necropsied. Mammary tumors were collected, snap frozen, and then sectioned at 8 μm thickness for staining or at 20 μm for AFM. All tissue sections were kept at −80°C until use.

Analysis of human breast tumor—To examine ESRP1 expression and distribution in human breast tumors and its correlation with ECM stiffness, tumor specimens from breast cancer patients were obtained from Cooperative Human Tissue Network according to the protocol approved by the Institutional Review Board at Vanderbilt University Medical Center (IRB No. 191552). Snap frozen breast tumors were sectioned at 8 μm thickness for staining or at 20 μm for AFM.

METHOD DETAILS

ESRP1 overexpression and shRNA-mediated knockdown of MENA and MENA^{11a}—For knockdown experiments, MDA-MB-231 cells were transduced with either PLKO shRNA scrambled control plasmid (#1864, Addgene, Watertown, MA, USA) or MENA shRNA oligonucleotides (5′-CAGAAGACAATCGCCCTTTAA-3′),[54] or MENA^{11a} shRNA oligonucleotides (5′-CATGATTCATTACACAGACCAA-3′).[7] For ESRP1 overexpression, MDA-MB-231 cells were transduced with either FUW empty vector or FUW vector with ESRP1 cDNA inserted. PLKO-shMENA, PLKO-shMENA^{11a}, and FUW-ESRP1 were generated by inserting shRNA oligonucleotides or ESRP1 cDNA into the PLKO.1 vector or FUW vector. Lentivirus particles were produced by transfecting each plasmid together with lentiviral expression vectors and second-generation packing constructs (psPAX2 and pMD2.G) in TransIT-LT1 (Mirus, Madison, WI, USA) into HEK293T cells. Lentiviral particles were harvested, concentrated with Lenti-X Concentrator (TaKaRa, Mountain View, CA, USA), and then transduced into MDA-MB-231 cells in the presence of polybrene (Santa Cruz Biotechnology, Dallas, TX, USA). After transduction, cells were selected with puromycin. Knockdown and overexpression efficiency was confirmed with western blotting.

Collagen-coated polyacrylamide gel—Polyacrylamide (PA) substrates were polymerized as described previously.[55] PA gels with 1 kPa or 10 kPa stiffness were synthesized by mixing different ratios of acrylamide [40% (w/v) solution] and bis-acrylamide [2% (w/v) solution] in Milli-Q water and TEMED in 0.25 M HEPES buffer at pH 6. Polymerization was initiated by adding APS. Substrates were functionalized with N-6-[(acryloyl) amido]hexanoic acid, succi-nimidyl ester (N6), and subsequently covalently bound to 0.1 mg/mL type I collagen (Corning, Corning, NY, USA). Unreacted N6 was neutralized using 1:1000 ethanolamine in 50 mM HEPES solution at pH 8. PA gels were washed in PBS and stored at 4°C in PBS with 2% penicillin/streptomycin before use.

Nonenzymatic glycation of collagen—Type I collagen was isolated from rat tail tendons as described previously.[22] Non-enzymatic glycation was utilized to produce collagen matrices of similar density and pore size at different stiffness. To glycate collagen, 10 mg/mL collagen solutions in 0.1% sterile acetic acid were mixed with 0.3 M ribose to form solutions containing 0 or 100 mM ribose and incubated for 5 days at 4°C. Glycated collagen solutions were then polymerized by adding 1N NaOH in 10×PBS, HEPES, and

sodium bicarbonate to form 1.5 mg/mL collagen gels with 1×PBS, 25 mM HEPES, and 44 mM sodium bicarbonate. Collagen was then incubated at 37°C for 1 h.

Intravasation-directed transendothelial migration model (iTEM)—Trans-well based iTEM model established previously was utilized to quantify tumor cell trans-endothelial migration from the subluminal side to the luminal side.[21] The underside of trans-well inserts was coated with glycated or unglycated collagen to achieve varying stiffness. After collagen polymerization, 100,000 HUVECs were seeded on the underside of the transwells and then flipped onto a 24-well plate containing 200 μL of M199 media supplemented with EGM SingleQuot Kit and incubated until endothelium monolayers formed. To mimic a physiologically relevant environment, all the assays were run in the presence of BAC1.2F5 murine macrophage cell line as described previously.[21] 15,000 BAC1.2F5 macrophages and 37,500 control or modified MDA-MB-231 cells were labeled with cell trackers respectively (Thermo Fisher Scientific), then embedded in glycated or unglycated collagen within the upper chamber of trans-wells. The thickness of the collagen matrix is around 900 μm. To achieve the serum gradient, the top of transwells was fed with DMEM/F12 supplemented with 0.5% FBS and 3000 Units of CSF-1, the bottom of trans-wells was fed with DMEM/F12 supplemented with 10% FBS and 3000 Units of CSF-1. After four days of co-culturing, transmigrated MDA-MB-231 cells were collected from the bottom of the plate and counted. Intravasation index was then obtained by dividing the number of cells collected by the number of cells seeded and normalized to cell proliferation rate of cell in each condition.

Quantitative reverse transcription PCR—MDA-MB-231 or MDA-MB-231 transduced with plasmids were cultured on PA gels for 24 h, rinsed with PBS, and collected after being treated with 0.5% trypsin. Cells were then pelleted, rinsed with PBS, and lysed with RLT buffer supplemented with β-Mercaptoethanol (MilliporeSigma). Total RNA was extracted using RNeasy Plus Kit (Qiagen Sciences, Germantown, MD, USA). Tumor RNA isolation was performed using a combination of TRIZOL (Invitrogen) and the RNeasy Mini Kit protocols. Briefly, snap-frozen tumors were homogenized in TRIZOL using the TissueLyserII (Qiagen) and a single 5 mm stainless steel bead (Qiagen). After homogenization, the lysates were incubated with an additional TRIZOL at room temperature and then added with chloroform. Samples were centrifuged at 12,000 ×g for 30 min at 4°C. The clear aqueous supernatant was carefully removed and placed into 70% ethanol. RNA extraction of samples was then performed using the RNeasy kit (Qiagen). After obtaining RNA from cell culture or tumors, 2 mg of total RNA per sample were then used to generate cDNA using the iScript kit (Bio-Rad). cDNAs were mixed with forward primer, reverse primer, and 1× iQ SYBR Green Supermix (BioRad) and analyzed with a My iQ Real-Time PCR Detection System (BioRad; see Table S1 for the primer sequences).[43,56] B2M was included as the housekeeping gene since its expression does not respond to the matrix stiffening.[57] The results were analyzed using the Livak method. Data were presented as an expression of the gene of interest relative to the expression of the housekeeping gene.

Western blotting—Snap frozen tumors extracted from mice were ground using a pre-cooled mortar and pestle and dissolved in Laemmli buffer. The lysate was collected and spun

at 14,000 ×g at 4°C for 10 min. The supernatant was collected and used for further analysis. Cells or cells transduced with plasmids were cultured on PA gels for 24 h before protein lysis. For pharmacologic treatment experiments, cells were treated with PF573228 or DMSO as vehicle control for 3 h before cell lysis. Total proteins were extracted with preheated 4× Laemmli buffer and stored at −80°C until use.[55] Protein concentration was measured with the DC Assay Kit (Bio-Rad). Protein samples were subjected to gel electrophoresis [8.5% (w/v) acrylamide gel] and western blotting. Membranes were blocked with either 5% milk or 5% BSA (MilliporeSigma) in TBS. Membranes were then incubated overnight with primary antibody at 4C, and secondary antibody for 1 h at room temperature. Primary antibodies were prepared at 1:40,000 dilution in 5% milk in the case of GAPDH (MAB374) or at 1:1000 dilution in 5% BSA in all other cases. Secondary antibodies were prepared at 1:2000 dilution. Membranes were imaged with West Pico, Dura, or Femto (Thermo Fisher Scientific) per their respective protocols using an ImageQuant LAS-4000 system. Quantification was performed with ImageJ (National Institutes of Health, NIH). The relevant protein expression level was expressed as the ratio of the protein of interest to GAPDH.

Immunofluorescence—In cases of MENA and YAP/TAZ staining, MDA-MB-231 on PA gels and tumor sections were fixed with 4% (v/v) paraformaldehyde, washed with PBS, and permeabilized with 1% (v/v) Triton X-100 in PBS. In cases of ESRP1-nucleus co-localization assay, cells or tissue sections were fixed and permeabilized by incubating samples in a pre-cooled 1:1 mixture of acetone and methanol for 20 min at −20°C. After fixation and permeabilization, all samples were blocked with 10% (v/v) FBS and 5% (v/v) donkey serum in PBS. Cells were stained with primary antibodies (anti-MENA, anti-ESRP1 antibody, anti-Ki67, or anti-YAP/TAZ) at 1:100 diluted in blocking solution overnight at 4C, washed with PBS supplemented with 0.02% Tween, and then incubated with secondary antibody (donkey anti-rabbit Alexa Fluor 488) at 1:200 diluted in blocking solution for 1 h at room temperature in the dark. Tissue samples were stained following the same procedure with the primary antibodies at 1:50 dilution and secondary antibodies at 1:100 dilution. For cell nucleus co-localization assay of ESRP1 or YAP/TAZ, the nucleus was stained with DAPI. For transwell staining, transwells were fixed, permeabilized, and blocked in the same way as described above, and incubated with anti-VE-cadherin primary antibodies at 1:100 diluted in blocking solution overnight at 4°C, washed with PBS, and then incubated with secondary antibody and phalloidin (A22283, Thermo Fisher Scientific) at 1:200 diluted in blocking solution for 1 h at room temperature in the dark. Immunofluorescent images were taken with a Zeiss LSM800 microscope using an x40/1.1 NA water immersion objective and 488 excitation laser line. Protein colocalization analysis was performed as described previously.[55] Cell area was measured using ImageJ.

Atomic force microscopy—Stiffness of tumor ECM was measured using contact mode atomic force microscopy (MFP-3D, Asylum Research, Goleta, CA). Snap frozen tissue samples at 20 μm thickness were stained for nuclei with Hoechst 33342 fluorescent stain (Thermo Fisher). The tissue area without positive nucleus signal was considered as ECM and was probed with a silicon nitride cantilever having a nominal spring constant of 0.06 N/m and 5 μm diameter borosilicate glass particle (Novascan, Boone, IA, USA). The spring constant of each probe was measured before use. Samples were incubated in

PBS supplemented with protease inhibitor cocktail (Thermo Fisher Scientific) during the measurement to avoid degradation. Force-displacement curves were obtained by indenting 2 or 3 force maps (10-by-10) on the tissue sections with an approach and retract speeds of 1 μm/s until reaching the maximum set force of 3 nN. The Young's modulus obtained from indention was extracted by fitting force-displacement curves to the Hertz model, assuming a Poisson's ratio of 0.5.

Quantitative polarization microscopy—Cell contractility was measured with quantitative polarization microscopy (qPOL) as described previously.[32] Images were acquired using a 20× polarization lens (NA = 0.5) with 5° intervals of the polarizer rotation over a range of 0–180°. The polarized image sequences were processed with a custom MATLAB code to obtain an optical retardance map. The retardance signal proportional to cell contractility was quantified by measuring the average retardance over the cell area after background subtraction.

Traction force microscopy—For traction force microscopy assays, cells were seeded on the 5 kPa PA gels embedded with 0.5 μm diameter fluorescent beads (Thermo Fisher Technology) and allowed to adhere for 24 h. Transmission images of each cells were then taken immediately followed by fluorescent images of the bead field at the gel surface. Cells were then removed with 0.25% (vol/vol) trypsin/EDTA (Thermo Fisher Technology) and a second fluorescent image of the bead field was captured. Bead displacements between the stressed and null state were calculated using the LIBTRC analysis library developed by M. Dembo (Dept. of Biomedical Engineering, Boston University). The overall traction force was quantified as described preisouly.[33]

Cell proliferation assay—Tumors extracted from mice treated with or without BAPN or MET-1 cells seeded on PA gel substrates with 1 kPa or 10 kPa stiffnesses and treated with BAPN for 3 days were fixed with 4% (v/v) paraformaldehyde in PBS for 10 min at room temperature. After fixation, samples were washed with PBS, permeabilized with 1% (v/v) Triton X-100 (Thermo Fisher Scientific) in PBS, blocked with 10% (v/v) fetal bovine serum (FBS), 5% (v/v) donkey serum, and 5% (v/v) goat serum for 2 h at room temperature. Samples were then stained with anti-Ki67 primary antibody at 1:100 diluted in PBS with 10% (v/v) FBS, 5% (v/v) donkey serum, and 5% (v/v) goat serum overnight at 4°C. After washing with PBS supplemented with 0.02% Tween, samples were then incubated with goat anti-rat Alexa Fluor 647 antibody (A21247; Thermo Fisher Scientific) at 1:100 diluted in PBS with 10% (v/v) FBS, 5% donkey serum, and 5% goat serum for 1 h at room temperature in the dark. Immunofluorescent images were acquired with a Zeiss LSM800 confocal microscope using a 40x/1.1 NA water immersion objective and 405, 568, and 640 excitation laser lines and z stack imaging. Protein colocalization analysis was performed as previously described.[58]

Cell migration assay—Control or genetically modified MDA-MB-231 cells were embedded in 1.5 mg/mL collagen gels glycated with or without 100 mM ribose. 3 h post embedding, cells were imaged using a Zeiss Axio Observer Z1 inverted microscope equipped with a Hamamatsu ORCA-ER camera and a 10×/0.3 NA objective and operated

by AxioVision software. Brightfield images were taken every 20 min across an 18-h period. Cells were kept at 37°C, 5% CO2, and 40% humidity during the imaging.[59] Average migration speed of each individual cell was measured using ImageJ and the MTrackJ plugin.

Monolayer permeability assay—iTEM models were set up as described previously.[21] The underside of trans-well inserts was coated with glycated or unglycated collagen and seeded with or without HUVECs. After formation of the endothelial monolayer, glycated or unglycated collagen without MDA-MB-231 cells and macrophages were polymerized within the upper chamber of trans-wells. Serum-free medium containing FITC-dextran solution (0.4 mg/mL 40 kDa) was added to the top of the transwell inserts. 50uL cell culture medium was collected from the bottom of the well every 20 min for 4 h. Fluorescence signal intensity of the collected medium was then quantified using a fluorescence plate reader (Infinite M1000 Pro, TECAN, Maännedorf, Switzerland). All datasets were fitted with a linear regression model. The computed slopes were calculated to represent the permeability of each sample[60]

The Cancer Genome Atlas (TCGA) breast cancer clinical dataset analyses—The results analyzed here are based upon data generated by the TCGA Research Network (https://www.cancer.gov/tcga) from breast invasive carcinoma [TCGA-BRCA] containing primary tumor samples from 1093 individual patients. Alternative splicing information in the form of specific exon read counts (GRCh37/hg19) of the ENAH gene were obtained from the TCGA Splicing Variation Database (http://www.tsvdb.com/index.html).[61] Additional clinical data and RNA-seq read counts for gene expression were downloaded from the TCGA database. Patient samples with low KRT8 gene expression (<3000 reads or 2.5% of all tumor samples) corresponding to stroma-biased samples were excluded. MENA^{11a} PSI values were calculated based on the ratio of exon 11a, and its flanking exons reads (chr1: 225688772–225692693, chr1: 225688772–225695653, chr1: 225692755–225695653).[62] Samples presenting low coverage of the ENAH gene or with a calculated MENA^{11a} PSI of 0 or 1 were further excluded from the analysis, yielding a dataset comprising 1066 patients. The YAP signature was generated based on 14 YAP-target genes (listed in Table S3).[36,37,63–65] A rank order list was generated based on the expression of each of the selected YAP responding genes using rank transformation. Each patient's average rank was then calculated to evaluate the YAP signature. The control signature was generated by calculating the average rank from 15 randomly selected genes (listed in Table S3).[66] All datasets were fitted with a linear regression model. The computed slopes were tested if they were significantly different from zero.

QUANTIFICATION AND STATISTICAL ANALYSIS

Statistical analysis was performed with GraphPad Prism 8.0a (GraphPad Software, La Jolla, CA, USA). All data are presented as means ± standard deviation (s.d.). Parametric one-way analysis of variance (ANOVA) followed by a post-hoc Tukey's Honest Significant Difference test was used where appropriate. Statistical significance was considered as $p < 0.05$.

Supplementary Material

Refer to Web version on PubMed Central for supplementary material.

ACKNOWLEDGMENTS

We would like to thank Dr. Richard Stanley for providing the BAC1.2F5 cell line. We thank Dr. Lauren A. Hapach for helpful reading of the manuscript. This work was supported in part by NIH grants HL127499 and GM131178 and an award from the W.M. Keck Foundation to C.A.R.-K.; CIHR project grant PLL-179768 and a Cancer Research Society Next Generation of Scientists Award to F.B.; AHA Predoctoral Fellowship (917613) and NCI Predoctoral to Postdoctoral Fellow Transition Award (1F99CA274695-01) to W.W.; F31 NHLBI Predoctoral Individual National Research Service Award (under grant no. 1F31HL154727) to P.V.T.; T32 Fellowship Award (under grant no. DK101003) to trainee K.S.; and an RQ-S doctoral training award to M.M. F.B. is a tier 2 Canada Research Chair in tumor mechanobiology and cellular mechanoregulation.

INCLUSION AND DIVERSITY

We support inclusive, diverse, and equitable conduct of research.

REFERENCES

1. Chiang SPH, Cabrera RM, and Segall JE (2016). Tumor cell intravasation. Am. J. Physiol. Cell Physiol. 311, C1–C14. 10.1152/ajpcell.00238.2015. [PubMed: 27076614]
2. Levental KR, Yu H, Kass L, Lakins JN, Egeblad M, Erler JT, Fong SFT, Csiszar K, Giaccia A, Weninger W, et al. (2009). Matrix crosslinking forces tumor progression by enhancing integrin signaling. Cell 139, 891–906. 10.1016/j.cell.2009.10.027. [PubMed: 19931152]
3. Pathak A, and Kumar S (2013). Transforming potential and matrix stiffness co-regulate confinement sensitivity of tumor cell migration. Integr. Biol. (Camb.) 5, 1067–1075. 10.1039/c3ib40017d. [PubMed: 23832051]
4. Fattet L, Jung HY, Matsumoto MW, Aubol BE, Kumar A, Adams JA, Chen AC, Sah RL, Engler AJ, Pasquale EB, and Yang J (2020). Matrix rigidity controls epithelial-mesenchymal plasticity and tumor metastasis via a mechanoresponsive EPHA2/LYN complex. Dev. Cell 54, 302–316.e7. 10.1016/j.devcel.2020.05.031. [PubMed: 32574556]
5. Wei SC, Fattet L, Tsai JH, Guo Y, Pai VH, Majeski HE, Chen AC, Sah RL, Taylor SS, Engler AJ, and Yang J (2015). Matrix stiffness drives epithelial-mesenchymal transition and tumour metastasis through a TWIST1-G3BP2 mechanotransduction pathway. Nat. Cell Biol. 17, 678–688. 10.1038/ncb3157. [PubMed: 25893917]
6. Oudin MJ, and Gertler FB (2017). Signatures of breast cancer metastasis: aMENAble to interpretation? Trends Cancer 3, 7–9. 10.1016/j.trecan.2016.11.004. [PubMed: 28718427]
7. Balsamo M, Mondal C, Carmona G, McClain LM, Riquelme DN, Tadros J, Ma D, Vasile E, Condeelis JS, Lauffenburger DA, and Gertler FB (2016). The alternatively-included 11a sequence modifies the effects of Mena on actin cytoskeletal organization and cell behavior. Sci. Rep. 6, 35298. 10.1038/srep35298. [PubMed: 27748415]
8. Di Modugno F, Mottolese M, Di Benedetto A, Conidi A, Novelli F, Perracchio L, Venturo I, Botti C, Jager E, Santoni A, et al. (2006). The cytoskeleton regulatory protein hMena (ENAH) is overexpressed in human benign breast lesions with high risk of transformation and human epidermal growth factor receptor-2–positive/hormonal receptor–negative tumors. Clin. Cancer Res. 12, 1470–1478. [PubMed: 16533770]
9. Forse CL, Agarwal S, Pinnaduwage D, Gertler F, Condeelis JS, Lin J, Xue X, Johung K, Mulligan AM, Rohan TE, et al. (2015). Mena calc, a quantitative method of metastasis assessment, as a prognostic marker for axillary node-negative breast cancer. BMC Cancer 15, 483. [PubMed: 26112005]
10. Berger AJ, Renner CM, Hale I, Yang X, Ponik SM, Weisman PS, Masters KS, and Kreeger PK (2020). Scaffold stiffness influences breast cancer cell invasion via EGFR-linked Mena upregulation and matrix remodeling. Matrix Biol. 85–86, 80–93. 10.1016/j.matbio.2019.07.006.

11. Gertler F, and Condeelis J (2011). Metastasis: tumor cells becoming MENAcing. Trends Cell Biol. 21, 81–90. 10.1016/j.tcb.2010.10.001. [PubMed: 21071226]
12. Roussos ET, Goswami S, Balsamo M, Wang Y, Stobezki R, Adler E, Robinson BD, Jones JG, Gertler FB, Condeelis JS, and Oktay MH (2011). Mena invasive (Mena(INV)) and Mena11a isoforms play distinct roles in breast cancer cell cohesion and association with TMEM. Clin. Exp. Metastasis 28, 515–527. 10.1007/s10585-011-9388-6. [PubMed: 21484349]
13. Di Modugno F, Iapicca P, Boudreau A, Mottolese M, Terrenato I, Perracchio L, Carstens RP, Santoni A, Bissell MJ, et al. (2012). Splicing program of human MENA produces a previously undescribed isoform associated with invasive, mesenchymal-like breast tumors. Proc. Natl. Acad. Sci. USA 109, 19280–19285. 10.1073/pnas.1214394109. [PubMed: 23129656]
14. Bear JE, Svitkina TM, Krause M, Schafer DA, Loureiro JJ, Strasser GA, Maly IV, Chaga OY, Cooper JA, Borisy GG, et al. (2002). Antagonism between Ena/VASP proteins and actin filament capping regulates fibroblast motility. Cell 109, 509–521. [PubMed: 12086607]
15. Mondal C (2016). Mena 11a-Isoform Specific Regulation of Actin Cytoskeleton Organization and Cell Behavior (Massachusetts Institute of Technology).
16. Agarwal S, Gertler FB, Balsamo M, Condeelis JS, Camp RL, Xue X, Lin J, Rohan TE, and Rimm DL (2012). Quantitative assessment of invasive mena isoforms (Mena calc) as an independent prognostic marker in breast cancer. Breast Cancer Res. 14, R124. [PubMed: 22971274]
17. Warzecha CC, and Carstens RP (2012). Complex Changes in Alternative Pre-mRNA Splicing Play a Central Role in the Epithelial-To-Mesenchymal Transition (EMT) (Elsevier), pp. 417–427.
18. Warzecha CC, Jiang P, Amirikian K, Dittmar KA, Lu H, Shen S, Guo W, Xing Y, and Carstens RP (2010). An ESRP-regulated splicing programme is abrogated during the epithelial–mesenchymal transition. EMBO J. 29, 3286–3300. [PubMed: 20711167]
19. Bordeleau F, Califano JP, Negrón Abril YL, Mason BN, LaValley DJ, Shin SJ, Weiss RS, and Reinhart-King CA (2015). Tissue stiffness regulates serine/arginine-rich protein-mediated splicing of the extra domain B-fibronectin isoform in tumors. Proc. Natl. Acad. Sci. USA 112, 8314–8319. [PubMed: 26106154]
20. Leight JL, Wozniak MA, Chen S, Lynch ML, and Chen CS (2012). Matrix rigidity regulates a switch between TGF-β1–induced apoptosis and epithelial–mesenchymal transition. Mol. Biol. Cell 23, 781–791. [PubMed: 22238361]
21. Pignatelli J, Goswami S, Jones JG, Rohan TE, Pieri E, Chen X, Adler E, Cox D, Maleki S, Bresnick A, et al. (2014). Invasive breast carcinoma cells from patients exhibit MenaINV-and macrophage-dependent transendothelial migration. Sci. Signal. 7, ra112. [PubMed: 25429076]
22. Mason BN, Starchenko A, Williams RM, Bonassar LJ, and Reinhart-King CA (2013). Tuning three-dimensional collagen matrix stiffness independently of collagen concentration modulates endothelial cell behavior. Acta Biomater. 9, 4635–4644. 10.1016/j.actbio.2012.08.007. [PubMed: 22902816]
23. Nenna A, Nappi F, Avtaar Singh SS, Sutherland FW, Di Domenico F, Chello M, and Spadaccio C (2015). Pharmacologic approaches against advanced glycation end products (AGEs) in diabetic cardiovascular disease. Res. Cardiovasc. Med. 4, e26949. 10.5812/cardiovascmed.4. [PubMed: 26393232]
24. Rowe MM, Wang W, Taufalele PV, and Reinhart-King CA (2022). AGE-breaker ALT711 reverses glycation-mediated cancer cell migration. Soft Matter 18, 8504–8513. [PubMed: 36325938]
25. Bordeleau F, Mason BN, Lollis EM, Mazzola M, Zanotelli MR, Somasegar S, Califano JP, Montague C, LaValley DJ, Huynh J, et al. (2017). Matrix stiffening promotes a tumor vasculature phenotype. Proc. Natl. Acad. Sci. USA 114, 492–497. 10.1073/pnas.1613855114. [PubMed: 28034921]
26. Pickup MW, Laklai H, Acerbi I, Owens P, Gorska AE, Chytil A, Aakre M, Weaver VM, and Moses HL (2013). Stromally derived Lysyl oxidase promotes metastasis of transforming growth factor-β–deficient mouse mammary CarcinomasStromal LOX promotes TGFβR2-null breast Cancer metastasis. Cancer Res. 73, 5336–5346. [PubMed: 23856251]
27. Nicolas-Boluda A, Vaquero J, Vimeux L, Guilbert T, Barrin S, Kantari-Mimoun C, Ponzo M, Renault G, Deptula P, Pogoda K, et al. (2021). Tumor stiffening reversion through collagen

crosslinking inhibition improves T cell migration and anti-PD-1 treatment. Elife 10, e58688. [PubMed: 34106045]

28. Yin H, Wang Y, Wu Y, Zhang X, Zhang X, Liu J, Wang T, Fan J, Sun J, Yang A, et al. (2020). EZH2-mediated epigenetic silencing of miR-29/miR-30 targets LOXL4 and contributes to tumorigenesis, metastasis, and immune microenvironment remodeling in breast cancer. Theranostics 10, 8494–8512. [PubMed: 32754259]
29. Roh-Johnson M, Bravo-Cordero JJ, Patsialou A, Sharma VP, Guo P, Liu H, Hodgson L, and Condeelis J (2014). Macrophage contact induces RhoA GTPase signaling to trigger tumor cell intravasation. Oncogene 33, 4203–4212. 10.1038/onc.2013.377. [PubMed: 24056963]
30. Khuon S, Liang L, Dettman RW, Sporn PHS, Wysolmerski RB, and Chew T-L (2010). Myosin light chain kinase mediates transcellular intravasation of breast cancer cells through the underlying endothelial cells: a three-dimensional FRET study. J. Cell Sci. 123, 431–440. [PubMed: 20067998]
31. Leerberg JM, Gomez GA, Verma S, Moussa EJ, Wu SK, Priya R, Hoffman BD, Grashoff C, Schwartz MA, and Yap AS (2014). Tension-sensitive actin assembly supports contractility at the epithelial zonula adherens. Curr. Biol. 24, 1689–1699. [PubMed: 25065757]
32. Wang W, Miller JP, Pannullo SC, Reinhart-King CA, and Bordeleau F (2018). Quantitative assessment of cell contractility using polarized light microscopy. J. Biophotonics 11, e201800008. [PubMed: 29931742]
33. Reinhart-King CA, Dembo M, and Hammer DA (2005). The dynamics and mechanics of endothelial cell spreading. Biophys. J. 89, 676–689. [PubMed: 15849250]
34. Bae YH, Mui KL, Hsu BY, Liu S-L, Cretu A, Razinia Z, Xu T, Puré E, and Assoian RK (2014). A FAK-Cas-Rac-lamellipodin signaling module transduces extracellular matrix stiffness into mechanosensitive cell cycling. Sci. Signal. 7, ra57. [PubMed: 24939893]
35. Slack-Davis JK, Martin KH, Tilghman RW, Iwanicki M, Ung EJ, Autry C, Luzzio MJ, Cooper B, Kath JC, Roberts WG, and Parsons JT (2007). Cellular characterization of a novel focal adhesion kinase inhibitor. J. Biol. Chem. 282, 14845–14852. 10.1074/jbc.M606695200. [PubMed: 17395594]
36. Dupont S, Morsut L, Aragona M, Enzo E, Giulitti S, Cordenonsi M, Zanconato F, Le Digabel J, Forcato M, Bicciato S, et al. (2011). Role of YAP/TAZ in mechanotransduction. Nature 474, 179–183. 10.1038/nature10137. [PubMed: 21654799]
37. Nardone G, Oliver-De La Cruz J, Vrbsky J, Martini C, Pribyl J, Skládal P, Pesl M, Caluori G, Pagliari S, Martino F, et al. (2017). YAP regulates cell mechanics by controlling focal adhesion assembly. Nat. Commun. 8, 15321. 10.1038/ncomms15321. [PubMed: 28504269]
38. Jaramillo-Rodrıguez Y, Cerda-Flores RM, Ruiz-Ramos R, López-Márquez FC, and Calderón-Garcidueñas AL (2014). YAP expression in normal and neoplastic breast tissue: an immunohistochemical study. Arch. Med. Res. 45, 223–228. [PubMed: 24606817]
39. Lee JY, Chang JK, Dominguez AA, Lee H-P, Nam S, Chang J, Varma S, Qi LS, West RB, and Chaudhuri O (2019). YAP-independent mechanotransduction drives breast cancer progression. Nat. Commun. 10, 1848. [PubMed: 31015465]
40. Wang Y, Zheng XR, Riddick N, Bryden M, Baur W, Zhang X, and Surks HK (2009). ROCK isoform regulation of myosin phosphatase and contractility in vascular smooth muscle cells. Circ. Res. 104, 531–540. 10.1161/CIRCRESAHA.108.188524. [PubMed: 19131646]
41. Ondeck MG, Kumar A, Placone JK, Plunkett CM, Matte BF, Wong KC, Fattet L, Yang J, and Engler AJ (2019). Dynamically stiffened matrix promotes malignant transformation of mammary epithelial cells via collective mechanical signaling. Proc. Natl. Acad. Sci. USA 116, 3502–3507. 10.1073/pnas.1814204116. [PubMed: 30755531]
42. Harvey SE, Xu Y, Lin X, Gao XD, Qiu Y, Ahn J, Xiao X, and Cheng C (2018). Coregulation of alternative splicing by hnRNPM and ESRP1 during EMT. RNA 24, 1326–1338. [PubMed: 30042172]
43. Ishii H, Saitoh M, Sakamoto K, Kondo T, Katoh R, Tanaka S, Motizuki M, Masuyama K, and Miyazawa K (2014). Epithelial splicing regulatory proteins 1 (ESRP1) and 2 (ESRP2) suppress cancer cell motility via different mechanisms. J. Biol. Chem. 289, 27386–27399. 10.1074/jbc.M114.589432. [PubMed: 25143390]

44. Gligorijevic B, Wyckoff J, Yamaguchi H, Wang Y, Roussos ET, and Condeelis J (2012). N-WASP-mediated invadopodium formation is involved in intravasation and lung metastasis of mammary tumors. J. Cell Sci. 125, 724–734. [PubMed: 22389406]
45. Warzecha CC, Shen S, Xing Y, and Carstens RP (2009). The epithelial splicing factors ESRP1 and ESRP2 positively and negatively regulate diverse types of alternative splicing events. RNA Biol. 6, 546–562. 10.4161/rna.6.5.9606. [PubMed: 19829082]
46. Rice AJ, Cortes E, Lachowski D, Cheung BCH, Karim SA, Morton JP, and Del Río Hernández A (2017). Matrix stiffness induces epithelial-mesenchymal transition and promotes chemoresistance in pancreatic cancer cells. Oncogenesis 6, e352. 10.1038/oncsis.2017.54. [PubMed: 28671675]
47. Cox TR, and Erler JT (2011). Remodeling and homeostasis of the extracellular matrix: implications for fibrotic diseases and cancer. Dis. Model. Mech. 4, 165–178. 10.1242/dmm.004077. [PubMed: 21324931]
48. Gargalionis AN, Basdra EK, and Papavassiliou AG (2018). Tumor mechanosensing and its therapeutic potential. J. Cell. Biochem. 119, 4304–4308. 10.1002/jcb.26786. [PubMed: 29479734]
49. Zhou W, Liu X, van Wijnbergen JWM, Yuan L, Liu Y, Zhang C, and Jia W (2020). Identification of PIEZO1 as a potential prognostic marker in gliomas. Sci. Rep. 10, 16121. [PubMed: 32999349]
50. Girard CA, Lecacheur M, Ben Jouira R, Berestjuk I, Diazzi S, Prod'homme V, Mallavialle A, Larbret F, Gesson M, Schaub S, et al. (2020). A feed-forward mechanosignaling loop confers resistance to therapies targeting the MAPK pathway in BRAF-mutant melanoma. Cancer Res. 80, 1927–1941. 10.1158/0008-5472.CAN-19-2914. [PubMed: 32179513]
51. Joyce MH, Lu C, James ER, Hegab R, Allen SC, Suggs LJ, and Brock A (2018). Phenotypic basis for matrix stiffness-dependent chemoresistance of breast cancer cells to doxorubicin. Front. Oncol. 8, 337. 10.3389/fonc.2018.00337. [PubMed: 30234012]
52. Maddipati R, Norgard RJ, Baslan T, Rathi KS, Zhang A, Saeid A, Higashihara T, Wu F, Kumar A, Annamalai V, et al. (2022). MYC levels regulate metastatic heterogeneity in pancreatic adenocarcinoma. Cancer Discov. 12, 542–561. [PubMed: 34551968]
53. Pisano M, Triacca V, Barbee KA, and Swartz MA (2015). An in vitro model of the tumor–lymphatic microenvironment with simultaneous transendothelial and luminal flows reveals mechanisms of flow enhanced invasion. Integr. Biol. 7, 525–533.
54. Oudin MJ, Barbier L, Schäfer C, Kosciuk T, Miller MA, Han S, Jonas O, Lauffenburger DA, and Gertler FB (2017). MENA confers resistance to paclitaxel in triple-negative breast cancer. Mol. Cancer Ther. 16, 143–155. 10.1158/1535-7163.MCT-16-0413. [PubMed: 27811011]
55. Wang W, Lollis EM, Bordeleau F, and Reinhart-King CA (2019). Matrix stiffness regulates vascular integrity through focal adhesion kinase activity. FASEB J. 33, 1199–1208. 10.1096/fj.201800841R. [PubMed: 30102569]
56. Patsialou A, Bravo-Cordero JJ, Wang Y, Entenberg D, Liu H, Clarke M, and Condeelis JS (2013). Intravital multiphoton imaging reveals multicellular streaming as a crucial component of in vivo cell migration in human breast tumors. Intravital 2, e25294. [PubMed: 25013744]
57. Chen G, Zhao L, Feng J, You G, Sun Q, Li P, Han D, and Zhou H (2013). Validation of reliable reference genes for real-time PCR in human umbilical vein endothelial cells on substrates with different stiffness. PLoS One 8, e67360. 10.1371/journal.pone.0067360. [PubMed: 23840676]
58. Huynh J, Nishimura N, Rana K, Peloquin JM, Califano JP, Montague CR, King MR, Schaffer CB, and Reinhart-King CA (2011). Age-related intimal stiffening enhances endothelial permeability and leukocyte transmigration. Sci. Transl. Med. 3, 112ra122. 10.1126/scitranslmed.3002761.
59. Mosier JA, Rahman-Zaman A, Zanotelli MR, VanderBurgh JA, Bordeleau F, Hoffman BD, and Reinhart-King CA (2019). Extent of cell confinement in microtracks affects speed and results in differential matrix strains. Biophys. J. 117, 1692–1701. [PubMed: 31623884]
60. Martins-Green M, Petreaca M, and Yao M (2008). An assay system for in vitro detection of permeability in human "endothelium". Methods Enzymol. 443, 137–153. [PubMed: 18772015]
61. Sun W, Duan T, Ye P, Chen K, Zhang G, Lai M, and Zhang H (2018). TSVdb: a web-tool for TCGA splicing variants analysis. BMC Genom. 19, 405. 10.1186/s12864-018-4775-x.
62. Kovalak C, Donovan S, Bicknell AA, Metkar M, and Moore MJ (2021). Deep sequencing of pre-translational mRNPs reveals hidden flux through evolutionarily conserved alternative splicing nonsense-mediated decay pathways. Genome Biol. 22, 132. [PubMed: 33941243]

63. Wang Y, Xu X, Maglic D, Dill MT, Mojumdar K, Ng PKS, Jeong KJ, Tsang YH, Moreno D, Bhavana VH, et al. (2018). Comprehensive molecular characterization of the hippo signaling pathway in cancer. Cell Rep. 25, 1304–1317.e5. 10.1016/j.celrep.2018.10.001. [PubMed: 30380420]

64. Fernandez-L A, Northcott PA, Dalton J, Fraga C, Ellison D, Angers S, Taylor MD, and Kenney AM (2009). YAP1 is amplified and up-regulated in hedgehog-associated medulloblastomas and mediates Sonic hedgehog-driven neural precursor proliferation. Genes Dev. 23, 2729–2741. [PubMed: 19952108]

65. Stein C, Bardet AF, Roma G, Bergling S, Clay I, Ruchti A, Agarinis C, Schmelzle T, Bouwmeester T, Schübeler D, and Bauer A (2015). YAP1 exerts its transcriptional control via TEAD-mediated activation of enhancers. PLoS Genet. 11, e1005465. 10.1371/journal.pgen.1005465. [PubMed: 26295846]

66. Serra-Juhé C, Martos-Moreno GÁ, Bou de Pieri F, Flores R, González JR, Rodríguez-Santiago B, Argente J, and Pérez-Jurado LA (2017). Novel genes involved in severe early-onset obesity revealed by rare copy number and sequence variants. PLoS Genet. 13, e1006657. 10.1371/journal.pgen.1006657. [PubMed: 28489853]

Highlights

- ECM stiffness promotes tumor cell intravasation
- ECM stiffness regulates MENA splicing via downregulating ESRP1 expression
- ECM stiffness rules MENA expression and splicing *in vitro*, *in vivo*, and in patients

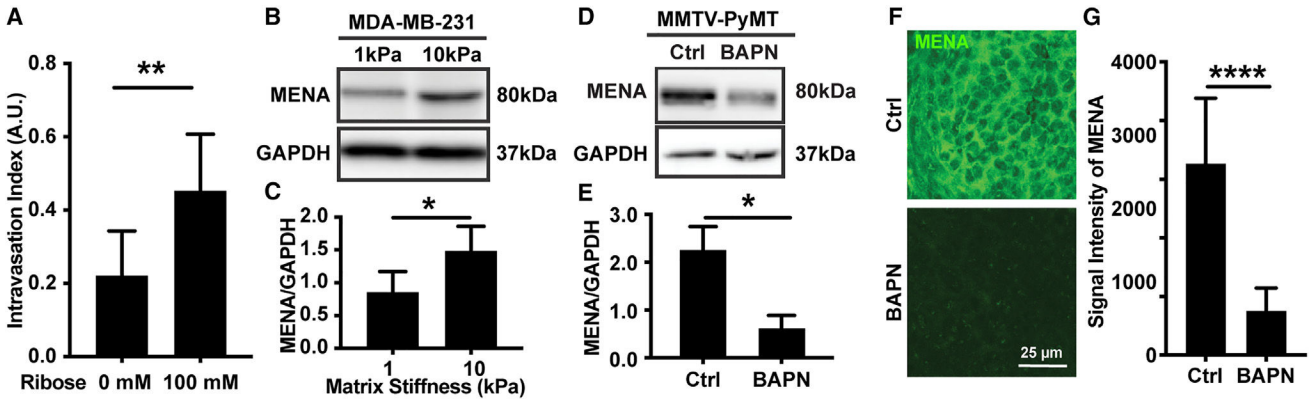

Figure 1. Matrix stiffness regulates MENA expression *in vitro* and *in vivo*

(A) Intravasation index of tumor cells embedded in collagen gels glycated with 0 or 100 mM ribose (N = 4).

(B and C) Western blot (B) and corresponding quantification (C) showing MENA expression in MDA-MB-231 cells seeded on PA gels with 1 or 10 kPa stiffness (N = 4).

(D and E) Protein bands generated by western blot (D) and corresponding quantification (E) showing MENA expression of breast tumors extracted from MMTV-PyMT mice treated with (BAPN) or without (Ctrl) BAPN (N = 5).

(F) Confocal microscopy images showing tumor sections of MMTV-PyMT mice treated with (BAPN) or with vehicle solution (Ctrl). Tumor sections were stained for MENA.

(G) Corresponding quantification of MENA signal intensity (n = 4; 10–15 imaging fields per condition for each experiment).

Data are presented as mean ± SD, *p < 0.05, **p < 0.01, ****p < 0.0001. (Scale bar, 25 μm)

See also Figures S1 and S2.

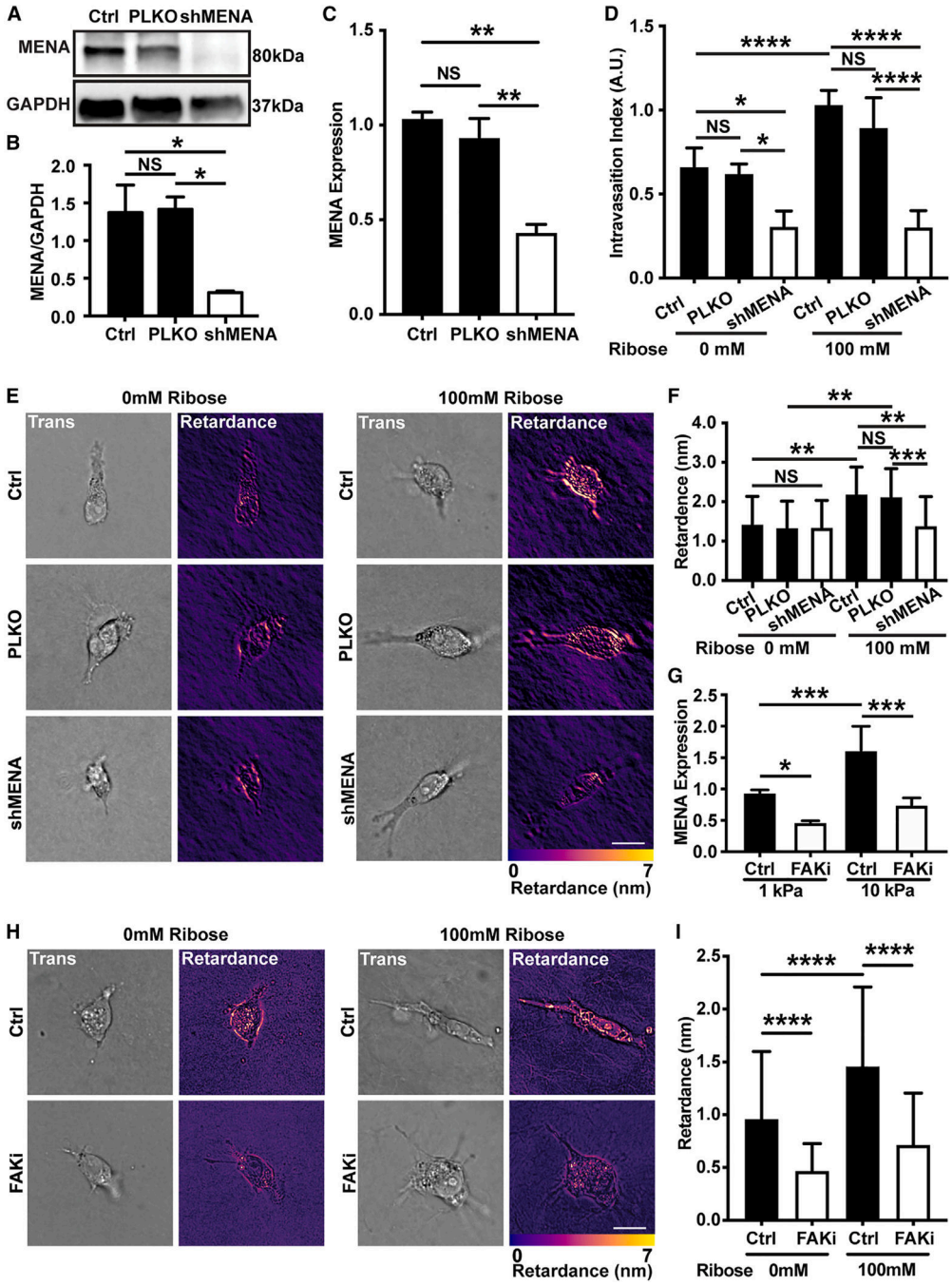

Figure 2. Matrix-stiffness-mediated MENA expression promotes tumor cell intravasation

(A and B) Western blot showing the knockdown efficiency of shRNA. Total MENA in MDA-MB-231 cells transduced with scrambled control shRNA (PLKO) or shRNA targeting MENA (shMENA) was assayed (N = 4).

(C) Quantitative RT-PCR showing MENA expression in MDA-MB-231 cells transduced with PLKO or shMENA, respectively (N = 3).

(D) Intravasation index of PLKO and shMENA cells embedded in collagen matrix glycated with 0 or 100 mM ribose (N = 3).

(E) Transmitted light (left) and computed retardance (right) images of PLKO or shMENA cells embedded in collagen matrix glycated with 0 or 100 mM ribose.
(F) Corresponding average retardance (N = 3, 70–72 cells per condition were included).
(G) Quantitative RT-PCR of MENA expression in MDA-MB-231 cells seeded on collagen-coated PA gels of 1 or 10 kPa stiffness treated with (FAKi) or without (Ctrl) PF573228, respectively (N = 3).
(H) Transmitted light (left) and computed retardance (right) images of MDA-MB-231 cells embedded in collagen matrix glycated with 0 or 100 mM ribose and treated with (FAKi) or without (Ctrl) PF573228.
(I) Corresponding average retardance (N = 3, 60–63 cells per condition).
Data are presented as mean ± SD, NS not significant, *p < 0.05, **p < 0.01, ***p < 0.001, ****p < 0.0001. (Scale bar, 25 μm).

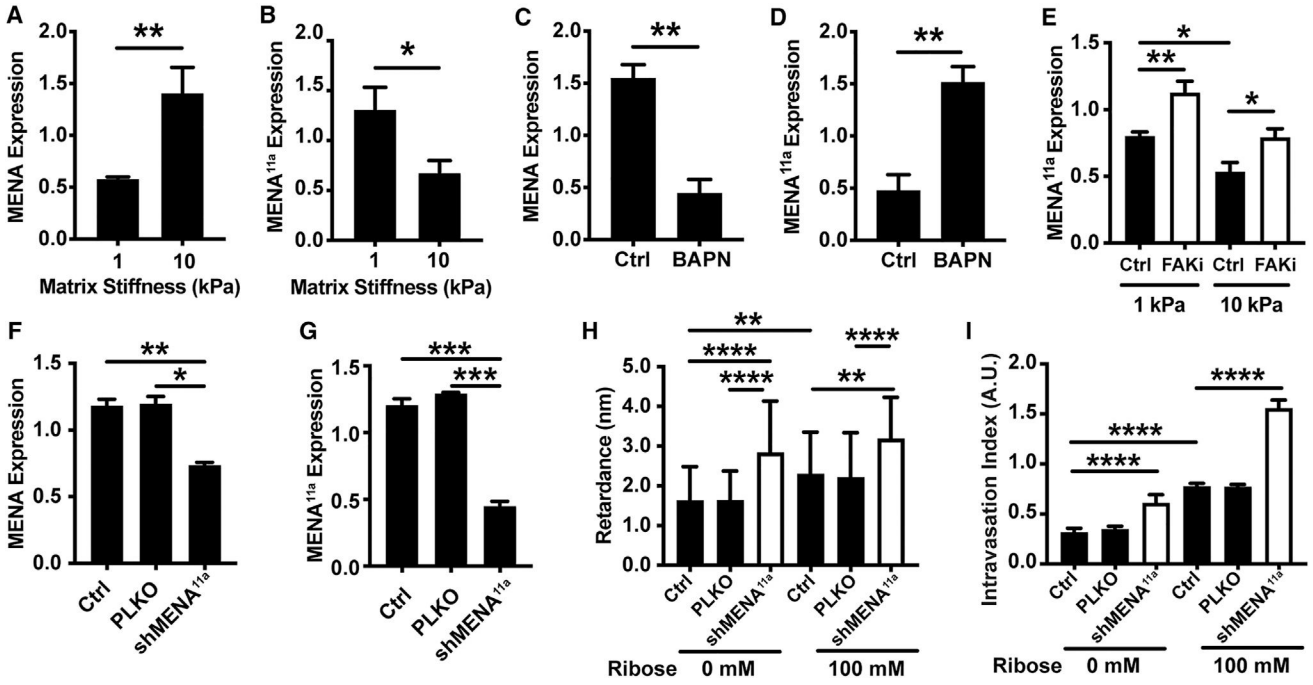

Figure 3. Matrix stiffening shifts alternative splicing of MENA, which further alters tumor cell intravasation

(A and B) Quantitative RT-PCR analysis of MENA (A) and MENA^{11a} (B) RNA expression in MDA-MB-231 cells seeded on 1 or 10 kPa PA gels (N = 3). (C and D) Quantitative RT-PCR analysis of MENA (C) and MENA^{11a} (D) expression within tumors extracted from the control group of PyMT mice (Ctrl) or the ones treated with BAPN (BAPN, N = 3).

(E) Quantitative RT-PCR analysis of MENA^{11a} RNA expression in MDA-MB-231 cells seeded on PA gels with different stiffnesses and treated with (FAKi) or without (Ctrl) PF573228 (N = 4).

(F and G) Quantitative RT-PCR analysis showing MENA (F) and MENA^{11a} (G) expression of MDA-MB-231 cells transduced with empty vector control or shRNA targeting MENA^{11a} (N = 3).

(H) Average retardance of control cells or cells transduced with scrambled control shRNA (PLKO) or shRNA targeting MENA^{11a} (shMENA^{11a}) and embedded in compliant (0 mM) or stiff (100 mM) collagen matrix (N = 3, 68–74 cells per condition were included).

(I) Intravasation index of PLKO and shMENA^{11a} cells embedded in collagen matrix glycated with 0 or 100 mM ribose (N = 3).

Data are presented as mean ± SD, *p < 0.05, **p < 0.01, ***p < 0.001, ****p < 0.0001. See also Figure S3.

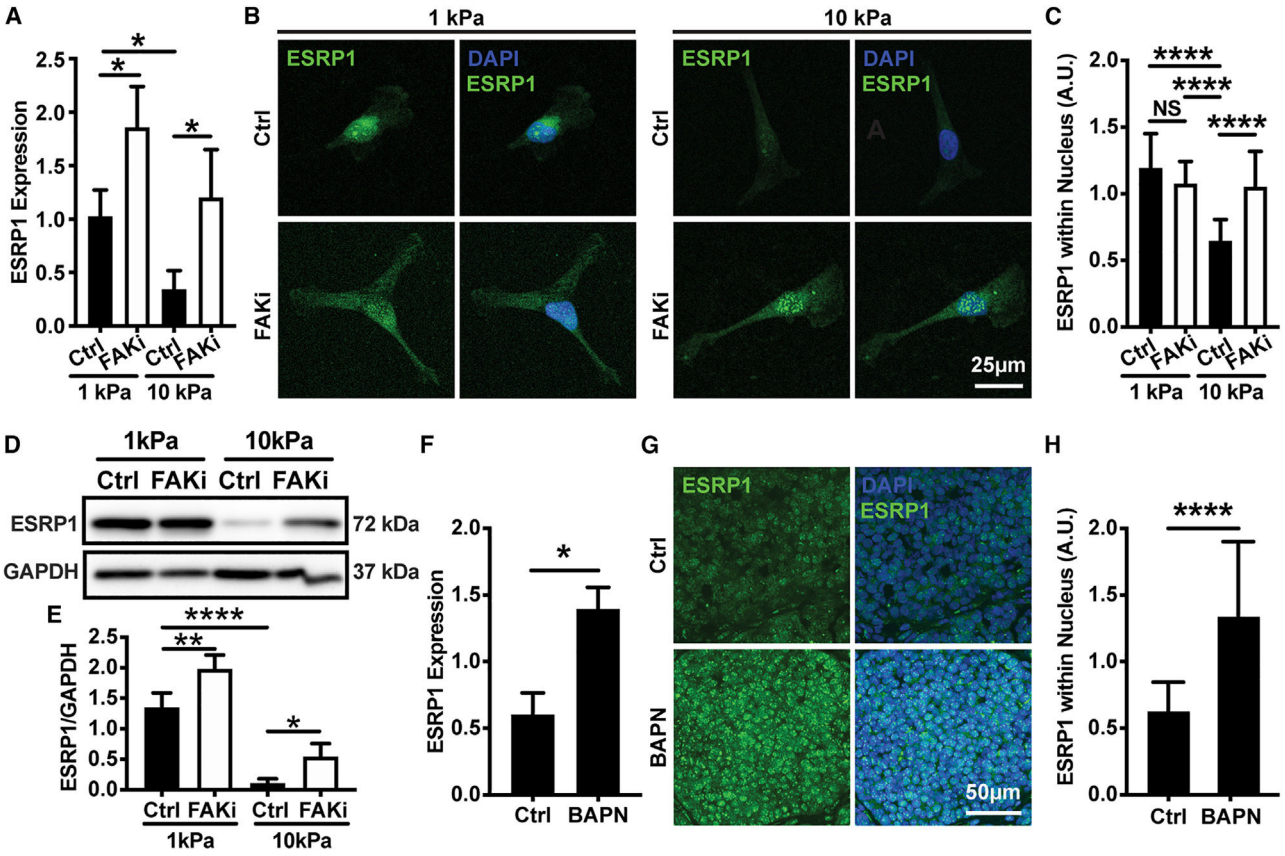

Figure 4. Matrix stiffening inhibits expression of ESRP1 and alters its localization within cells

(A) Quantitative RT-PCR analysis of ESRP1 RNA expression in MDA-MB-231 cells seeded on PA gels with 1 or 10 kPa stiffness and treated with (FAKi) or without (Ctrl) PF573228 (N = 4).

(B) Representative image showing ESRP1 within MDA-MB-231 cells seeded on compliant (1 kPa) or stiff (10 kPa) substrates treated with (FAKi) or without (Ctrl) PF573228. (Scale bar, 25 μm).

(C) Corresponding quantification of the amount of ESRP1 signal within the nucleus (N = 3, 15–18 imaging fields per condition).

(D and E) Western blot (D) and corresponding quantification (E) of ESRP1 expression in MDA-MB-231 cells seeded on 1 or 10 kPa PA gels and treated with (FAKi) or without (Ctrl) PF573228 (N = 4).

(F) Quantitative RT-PCR analysis of ESRP1 expression within tumors extracted from the control group of PyMT mice (Ctrl) or the ones treated with BAPN (BAPN, N = 3).

(G) Confocal images of tumor sections extracted from MMTV-PyMT mice treated with (BAPN) or without (Ctrl) BAPN. Tumor sections were stained for ESRP1 and nucleus. (Scale bar, 50 mm).

(H) Corresponding quantification of ESRP1 signal within nucleus showing matrix stiffening decreases ESRP1 and nucleus co-localization (n = 4; 10–13 imaging fields per condition for each experiment).

Data are presented as mean ± SD, NS not significant, *p < 0.05, ****p < 0.0001.

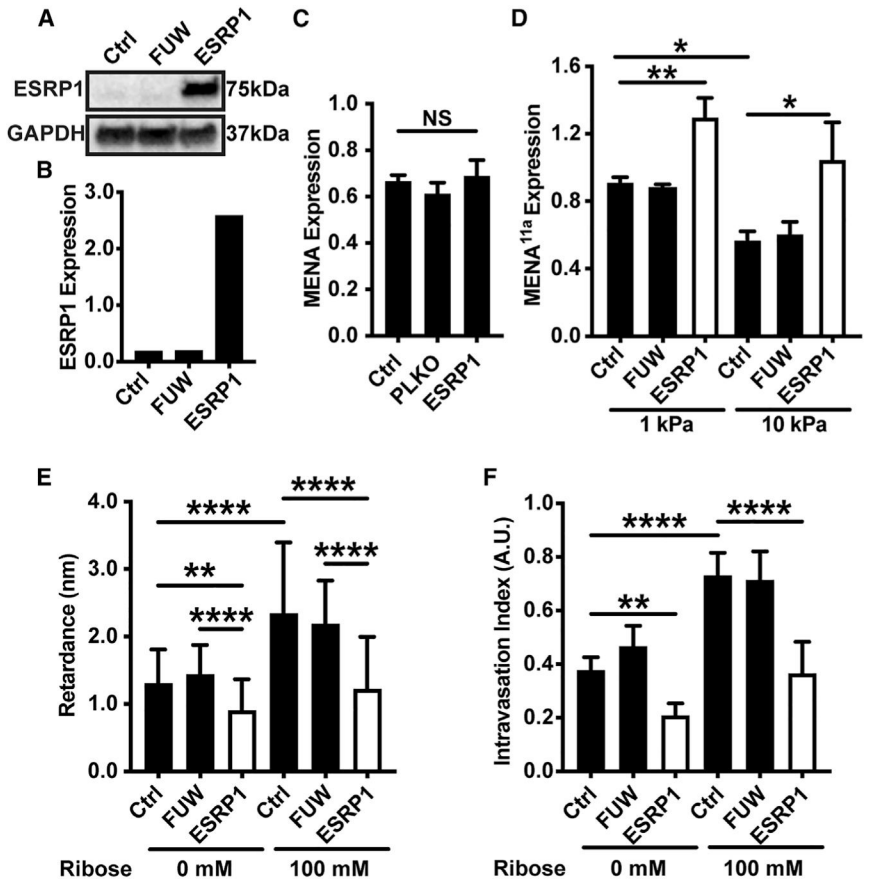

Figure 5. Matrix stiffness regulates alternative splicing of MENA through ESRP1

(A) Western blot showing ESRP1 expression ofMDA-MB-231 cells seeded on plastic and transduced with empty control vector (FUW) or ESRP1 overexpression vector (ESRP1).

(B) Corresponding quantification of ESRP1 expression normalized to GAPDH showing the overexpression of control and ESRP1 overexpressed MDA-MB-231 cells (N = 3).

(C) Quantitative RT-PCR analysis of MENA expression at the RNA level in MDA-MB-231 cells transduced with empty control vector (FUW) or ESRP1 overexpression vector (ESRP1) (N = 3).

(D) Quantitative RT-PCR analysis of $MENA^{11a}$ RNA expression in control cells or cells transduced with empty vector (FUW) or ESRP1 overexpression vector (ESRP1) and seeded on PA gels with 1 or 10 kPa stiffness (N = 3).

(E) Average retardance of control cells or cells transduced with empty vector (FUW) or ESRP1 overexpression vector (ESRP1) and embedded in compliant (0 mM) or stiff (100 mM) collagen matrix (N = 3, 68–71 cells per condition were included).

(F) Intravasation index of FUW and ESRP1 overexpression cells embedded in collagen matrix glycated with 0 or 100 mM ribose (N = 3).

Data are presented as mean ± SD, NS not significant, *p < 0.05, **p < 0.01, ****p < 0.0001.

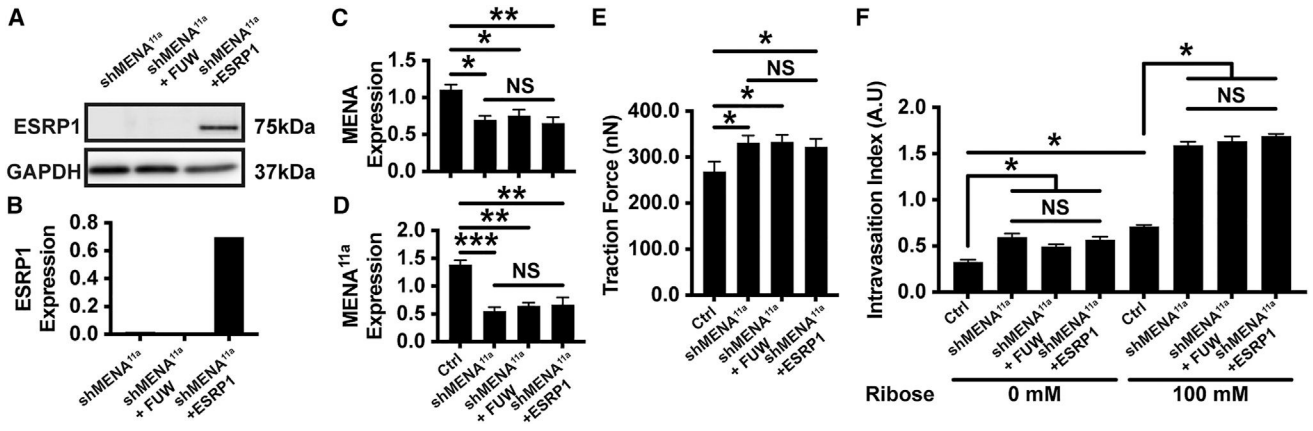

Figure 6. ESRP1 shifts alternative splicing of MENA, which regulates tumor cell intravasation

(A) Western blot showing ESRP1 expression of shMENA^{11a} cells transduced with empty control vector (shMENA^{11a} + FUW) or ESRP1 overexpression vector (shMENA^{11a} + ESRP1).

(B) Corresponding quantification of ESRP1 expression normalized to GAPDH showing the overexpression of control and ESRP1 overexpressed shMENA^{11a} cells.

(C) Quantitative RT-PCR analysis of MENA expression at the RNA level in shMENA^{11a} cells transduced with empty control vector (shMENA^{11a} + FUW) or ESRP1 overexpression vector (shMENA^{11a} + ESRP1) (N = 3).

(D) Quantitative RT-PCR analysis of MENA^{11a} RNA expression in shMENA^{11a} cells or cells transduced with empty vector (shMENA^{11a} + FUW) or ESRP1 overexpression vector (shMENA^{11a} + ESRP1) and seeded on PA gels with 1 or 10 kPa stiffness (N = 3).

(E) Average traction force of shMENA^{11a} cells or cells transduced with empty vector (shMENA^{11a} + FUW) or ESRP1 overexpression vector (shMENA^{11a} + ESRP1) (N = 3, 45–62 cells per condition were included).

(F) Intravasation index of FUW and ESRP1 overexpression shMENA^{11a} cells or cells transduced with empty vector (shMENA^{11a} + FUW) or ESRP1 overexpression vector shMENA^{11a} cells embedded in collagen matrix glycated with 0 or 100 mM ribose (N = 3).

Data are presented as mean ± SD, NS not significant, *p < 0.05, **p < 0.01, ***p < 0.001.

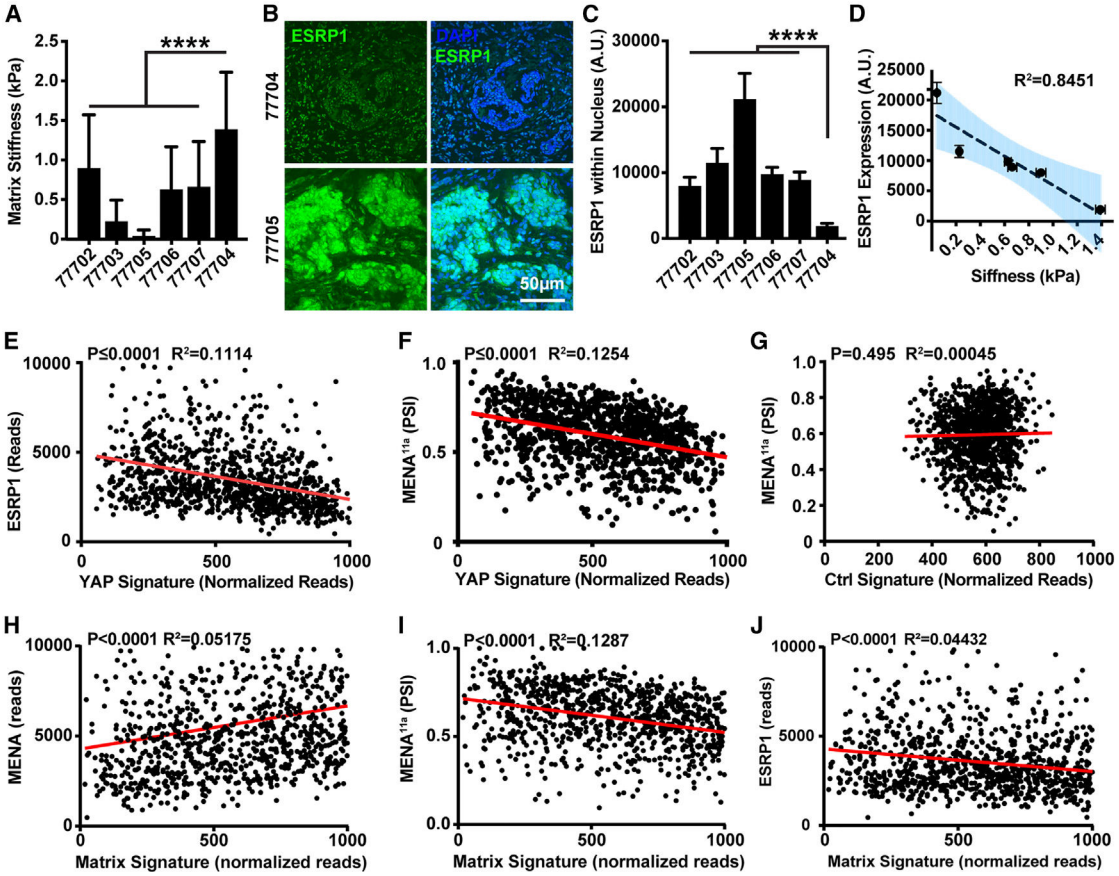

Figure 7. Matrix stiffening decreases ESRP1 expression of tumors from patients with breast cancer

(A) AFM measurement of tumor ECM stiffness. Tissue specimens were extracted from different patients (300–450 measurements per specimen).

(B) Confocal images of tumor sections extracted from patients with breast cancer. Tumor sections were stained for ESRP1 and nuclei.

(C) Corresponding quantification of ESRP1 signal within the nucleus (5–8 imaging fields per condition for each experiment).

(D) Scatterplot of the ESRP1 expression level of tumor specimens as a function of matrix stiffness of the tumor stroma.

(E) Scatterplot showing the negative correlation between the expression levels of ESRP1 and YAP signature genes in 1,093 patients with breast cancer in TCGA dataset.

(F) Scatterplot showing the negative correlation between MENA^{11a} percent spliced in and YAP signature genes in 1,066 patients with breast cancer in TCGA dataset.

(G) Scatterplot showing there is no correlation between MENA^{11a} percent spliced in and randomly selected control signature genes.

(H) Scatterplot showing the positive correlation between the expression levels of MENA and matrix signature genes in TCGA dataset.

(I) Scatterplot showing the negative correlation between MENA^{11a} percent spliced in and matrix signature genes in TCGA dataset.

(J) Scatterplot showing there is negative correlation between ESRP1 expression and matrix signature genes. The resulting data were fit with the linear regression (dash line) and confidence interval (95%). The p value deviation from 0 and R^2 value is provided.
Data are presented as mean ± SD, ****p < 0.0001. (Scale bar, 50 μm).
See also Figure S4 and Tables S2 and S3.

KEY RESOURCES TABLE

REAGENT or RESOURCE	SOURCE	IDENTIFIER	
Antibodies			
anti-MENA antibody	MilliporeSigma	RRID:AB_11214403	MAB2635
anti-rat Alexa Fluor 647 goat antibody	Thermo Fisher Scientific	RRID:AB_141778	A21247
anti-ESRP1 antibody	Abcam	RRID:AB_10862543	ab107278
anti-Ki67 antibody	Thermo Fisher Scientific	AB_10854564	14–5698-82
anti-YAP/TAZ	Cell Signaling technology	RRID:AB_10950494	8418
anti-VE-cadherin	Thermo Fisher Scientific	RRID:AB_842767	14–1441-82
anti-rabbit Alexa Fluor 568 donkey antibody	Thermo Fisher Scientific	RRID:AB_2534017	A10042
anti-glyceraldehyde-3-phosphate dehydrogenase antibody (GAPDH)	MilliporeSigma	RRID:AB_2107445	MAB374
anti-GAPDH antibody	BioLegend	N/A	Poly6314
horseradish peroxidase (HRP) conjugated pre-adsorbed anti-mouse IgG antibody	Rockland	RRID:AB_218457	610–103-121
HRP conjugated pre-adsorbed anti-rabbit IgG antibody	Rockland	RRID:AB_218567	611–103-122
Biological samples			
Tissue sections from breast cancer patients	Cooperative Human Tissue Network	N/A	
Chemicals, peptides, and recombinant proteins			
DMEM	Thermo Fisher Scientific	11965092	
a-MEM	Thermo Fisher Scientific	32561037	
DMEM/F12 media	Thermo Fisher Scientific	11320033	
M-199 media	Thermo Fisher Scientific	31150022	
penicillin-streptomycin	Thermo Fisher Scientific	10378016	
0.25% and 0.5% trypsin	Thermo Fisher Scientific	25200056	
EGM SingleQuot Kit	Lonza	204579	
FAK inhibitor (PF573228)	MilliporeSigma	PZ0117	
ammonium persulfate (APS)	Biorad	1610700EDU	
Acrylamide [40% (w/v) solution]	Biorad	1610140	
bis-acrylamide [2% (w/v) solution]	Biorad	1610142	
CSF-1	R&D System	216-MC	
Ribose	Thermo Fisher Scientific	132365000	
β-Mercaptoethanol	MilliporeSigma	444203	
TRIZOL	Invitrogen	15596026	
iQ SYBR Green Supermix	BioRad	1708880	
BSA	MilliporeSigma	A2153	
SuperSignal™ West Pico PLUS Chemiluminescent Substrate	Thermo Fisher Scientific	34580	
SuperSignal™ West Dura Extended Duration Substrate	Thermo Fisher Scientific	34075	
SuperSignal™ West Femto Maximum Sensitivity Substrate	Thermo Fisher Scientific	34095	
FITC-dextran (40 kDa)	MilliporeSigma	FD40	

REAGENT or RESOURCE	SOURCE	IDENTIFIER
3-Aminopropionitrilefumarate salt (BAPN)	MilliporeSigma	A3134
Critical commercial assays		
Universal mycoplasma detection kit	ATCC	30–1012K
RNeasy Plus Kit	Qiagen Sciences	74034
iScript kit	Bio-Rad	1708890
Experimental models: Cell lines		
Human umbilical vein endothelial cells (HUVECs)	LONZA	C2519A
Highly metastatic MDA-MB-231 breast adenocarcinoma cells	ATCC	CRM-HTB-26
HEK293T	ATCC	CRL-11268
MET-1 Cells	extracted from MMTV-PyMT mice	N/A
BAC1.2F5 cells	generously provided by Dr. Richard Stanley, Albert Einstein College of Medicine	N/A
Experimental models: Organisms/strains		
Mouse: FVB/N-Tg(MMTV-PyVT)634Mul/J (MMTV-PyMT)	Jackson Laboratory	002374
Oligonucleotides		
MENA shRNA oligonucleotides (5′-CAGAAGACAATCGCCCTTTAA-3′)	MilliporeSigma	N/A
MENA^{11a}shRNA oligonucleotides (5′ -CATGATTCATTACACAGACCAA-3′)	MilliporeSigma	N/A
ESRP1 Forward: 5′- CAA TAT TGC CAA GGG AG GTG -3′	MilliporeSigma	N/A
ESRP1 Reverse: 5′-GTC CCC ATG TGA TGT TTG TG-3′	MilliporeSigma	N/A
Human MENA Forward: 5′-AGG CTG AAG CAG GAC ATT TT-3′	MilliporeSigma	N/A
Human MENA Reverse: 5′-TGC TCA GTT CCT GCC TGA T-3′	MilliporeSigma	N/A
Mouse MENA Forward: 5′-CGG CAG TAA GTC ACC TGT CA-3′	MilliporeSigma	N/A
Mouse MENA Reverse: 5′-CTT CAG CTT TGC CAG CTC TT-3′	MilliporeSigma	N/A
MENA11a Forward: 5′- CCA ACC AGA AAA CCT TGG G-3′	MilliporeSigma	N/A
MENA11a Reverse: 5′-TGC TTC AGC CTC TCA TAG TCA-3′	MilliporeSigma	N/A
Human MENAINV Forward: 5′-AGA GGA TGC CAA TGT CTT CG-3′	MilliporeSigma	N/A
Human MENAINV Reverse: 5′-TTA GTG CTG TCC TGC GTA GC-3′	MilliporeSigma	N/A
Human MENADV6 Forward: 5′-GCT GGA ATG GGA GAG AGA GCG CAG AAT A-3′	MilliporeSigma	N/A
Human MENADV6 Reverse: 5′-GTT CAC ACC AAT AGC ATT CCC TCC ACT TG-3′	MilliporeSigma	N/A
B2M Forward: 5′-CAC CCC CAC TGA AAA AGA TGA G-3′	MilliporeSigma	N/A
B2M Reverse: 5′-CCTCCATGATGCTG CTTACATG-3′	MilliporeSigma	N/A
Software and algorithms		

REAGENT or RESOURCE	SOURCE	IDENTIFIER
GraphPad Prism 8.0a	GraphPad Software	N/A
ImageJ	National Institutes of Health	N/A